Signal Detection and Optimal Antenna Selection for Ambient Backscatter Communications With Multi-Antenna Tags

Chen Chen, Gongpu Wang, *Member, IEEE*, Panagiotis D. Diamantoulakis, *Senior Member, IEEE*, Ruisi He, *Senior Member, IEEE*, George K. Karagiannidis, *Fellow, IEEE*, and Chintha Tellambura, *Fellow, IEEE*

***Abstract*— Ambient backscatter devices (tags and readers) use existing radio frequency (RF) signals to transmit data. Most prior works consider single-antenna tags, but this paper investigates the case of multiple-antenna tags, which are capable of simultaneous energy harvesting and data transmission. However, the multi-antenna channel between the tag and the reader, and the unpredictable nature of RF signals due to uncontrollable RF sources (e.g., location and transmit power), make signal detection highly challenging. Thus, the detection process becomes a hypothesis testing problem with unknown parameters. Consequently, we design a blind detector based on the generalized likelihood ratio test (GLRT) without using channel state information (CSI), signal power and noise variance. The decision threshold and detection probability of it are also analyzed in detail. Furthermore, to maximize its detection performance, we develop the optimal backscatter antenna selection scheme. Interestingly, we show that the detector performs best when only two backscatter antennas are selected. Finally, extensive simulation results validate the analysis and illustrate the effectiveness of the proposed detector.**

***Index Terms*— Ambient backscatter, generalized likelihood ratio test, multiple antennas, probability of detection.**

I. Introduction

AMBIENT backscatter has recently emerged as a novel communication paradigm for the Internet-of-Things (IoT), which enables mutual communication among battery-free devices via backscattering radio frequency (RF) signals [1], [2]. Ambient RF signals are transmitted by existing RF sources, such as television (TV) towers, frequency modulation (FM) radio stations, cellular base stations, and Wi-Fi access points. Unlike conventional backscatter [3], ambient backscatter eliminates the need for dedicated infrastructure elements such as radio frequency identification (RFID) readers, dedicated power transmit blocks and others. Moreover, the sole reliance on existing ambient RF signals improves the utilization of the wireless spectrum, which is scarce and expensive.

First proposed in [2], the ambient scatter device harvests energy from TV signals and then transmits its own signals by switching its antenna impedance, which results in *reflecting* or *non-reflecting* states. In the *non-reflecting* state, representing bit '0', the RF signals are absorbed. In contrast, in the *reflecting* state, representing bit '1', the RF signals are backscattered. Reference [4] demonstrates that RF-powered devices can be connected to Internet by backscattering Wi-Fi signals. To achieve higher data transmission rate and sufficient communication range, full-duplex backscatter communications has been proposed in [5], while a novel multi-antenna cancellation and coding mechanism is developed in [6]. Passive Wi-Fi is introduced in [7] to directly generate Wi-Fi transmissions through backscatter communication that consumes much lower power than existing Wi-Fi devices. Other than TV and Wi-Fi signals, FM radio signals can also be used as an RF source to achieve backscatter communication in outdoor environments [8].

Moreover, fundamental theoretical results for ambient backscatter communication systems include channel estimation [9], signal detection [10]–[15], coding [16]–[18], collision avoidance [19]–[22], transmission and energy harvesting [23]–[26], multicast transmission [27]–[29], and performance analysis in terms of bit error rate (BER) and channel capacity [30]–[32]. Specifically, the problem of ambient-backscatter channel estimation when both reader and tag are single-antenna entities is studied in [9]. A new coding scheme has been designed in [18] by using manchester coding to reduce the communication delay. However, the design of space-time coding [33], [35] for ambient backscatter communication systems remains an open problem. Ambient backscatter systems with multiple tags and the corresponding tag selection strategies are also investigated [19]. To overcome

Manuscript received January 6, 2019; revised June 20, 2019 and August 29, 2019; accepted October 1, 2019. Date of publication October 10, 2019; date of current version January 15, 2020. This work was supported in part by the Fundamental Research Funds for the Central Universities under Grant 2018YJS026, and in part by the National Natural Science Foundation of China under Grant 61571037, Grant 61871026 and Grant 61922012. This paper was presented in part at the IEEE Globecom 2018 [53]. The associate editor coordinating the review of this article and approving it for publication was I. Krikidis. *(Corresponding author: Gongpu Wang.)*

C. Chen and G. Wang are with the Beijing Key Laboratory of Transportation Data Analysis and Mining, School of Computer and Information Technology, Beijing Jiaotong University, Beijing 100044, China (e-mail: 16120355@bjtu.edu.cn; gpwang@bjtu.edu.cn).

P. D. Diamantoulakis and G. K. Karagiannidis are with the Department of Electrical and Computer Engineering, Aristotle University of Thessaloniki, 54124 Thessaloniki, Greece (e-mail: padiaman@auth.gr; geokarag@auth.gr).

R. He is with the State Key Laboratory of Rail Traffic Control and Safety, Beijing Jiaotong University, Beijing 100044, China (e-mail: ruisi.he@bjtu.edu.cn).

C. Tellambura is with the Department of Electrical and Computer Engineering, University of Alberta, Edmonton, AB T6G 2V4, Canada (e-mail: chintha@ece.ualberta.ca).

Color versions of one or more of the figures in this article are available online at http://ieeexplore.ieee.org.

Digital Object Identifier 10.1109/TCOMM.2019.2946799

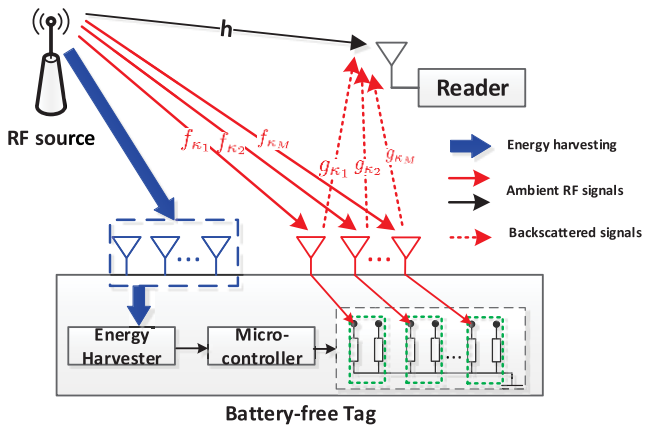

Fig. 1. The multi-antenna-tag ambient backscatter system. $K \in [2, 4]$.

the collisions caused by the multiple concurrent transmissions from multiple tags, a collision avoidance method is proposed in [21], based on antenna directionality and successive interference cancellation. Reference [20] introduces a new technique for energy beamforming in multi-tag backscatter communication systems. Furthermore, the integration of wireless power transfer (WPT) with low-power backscatter communications has been studied extensively for single-antenna tags. For example, [25] proposes a network architecture for WPT backscatter communications and analyzes the network coverage and capacity. A two-hop backscatter relay scheme and the joint optimization of wireless power transfer and relay strategy have been developed in [26].

Several signal detection schemes have also been investigated. In [10], a differential encoding scheme eliminates the requirement of channel estimation and enables the decoding of the tag information via signal power difference. The noncoherent signal detector for ambient backscatter [11] avoids channel state information (CSI) and training symbols, while the semi-coherent detector of [12] obtains channel-related parameters from unknown data symbols and a few pilot symbols. Finally, signal detection for ambient backscatter communication systems with multiple-antenna readers has been studied in [13] and [14].

A. Motivation

In the aforementioned works, the key assumption is that the tag has only a single antenna and that it is shared among the transmit, receive and energy harvesting functions of the tag. Thus, these operations are sequential. For example, the harvester collects energy from the ambient RF signals, which is then used to power the microcontroller and perform the backscatter communication. Consequently, during energy harvesting, the transmitter is silent and cannot deliver tag information. Similarly, when the tag is transmitting information, energy harvesting is not possible. To overcome this fundamental limitation, we propose the use of a tag with multiple antennas. The tag antennas (Fig. 1) are divided into two sets: one for energy harvesting and the other for backscatter modulation. Consequently, energy harvesting and backscatter communication can occur simultaneously. It is worth noting that multi-antenna tags add the benefits of extending coverage [34] and increasing communication reliability [35], compared to conventional backscatter communication systems with single-antenna tags.

However, since the use of multiple antennas between the tag and the reader increases the required overhead to estimate the channel parameters, and thus, it becomes a major challenge (see [43]–[45] and references therein). This is because the tag may only transmit a limited number of symbols to estimate the channel parameters, due to the strict energy constraints. In order to address this challenge, a modified energy detector has been introduced in [15], which can recover the signal from the multi-antenna tag without the knowledge of CSI between the tag and the reader. However, it still requires the knowledge of the RF signal power, noise variance, and CSI between the RF source and the reader. In practice, the parameters of ambient RF sources are not controllable (e.g., transmit power and location) and the ambient RF signals are random and unpredictable, which further complicate the detection of the backscattered information from the received signals. Consequently, a blind detector is needed in order to detect the information sent by the tag.

B. Contributions

In this paper, we address the problem of blind detection of ambient backscatter signals from a multi-antenna tag via the generalized likelihood ratio test (GLRT). Note that the hypothesis testing problem with unknown parameters is typically handled via GLRT or Bayesian approaches [46]. The main difference between them is how the unknown parameters get treated. The Bayesian approach requires their prior distribution; whereas GLRT requires their maximum likelihood estimates (MLEs).

The main contribution of this paper can be summarized as follows:

- We present two backscatter schemes at the tag, namely, a general backscatter scheme (GBS) and a specially designed backscatter scheme (SDBS). The GBS uses an arbitrary number of signals per antenna, while the SDBS uses a quantized number of signals per antenna.
- For the SDBS, we design a GLRT based detector, which forms the decision statistic from the eigenvalues of the covariance matrix of the received signals at the reader.
- We derive an approximate decision threshold and the detection probability of the GLRT based detector with the SDBS.
- We propose an optimal backscatter antenna selection scheme to maximize the detection probability.

C. Structure

The paper is organized as follows. Section II presents the GBS of the multiple-antenna tag and the theoretical model for ambient backscatter communications with such tags. Section III proposes the GLRT based detectors with GBS and SDBS, respectively, while a modified energy detector is also given for comparison purposes. Section IV investigates the

optimal backscatter antenna selection scheme, that maximizes the detection probability. Finally, simulation results are provided in Section V and conclusions are drawn in Section VI.

D. Notations

Scalars, vectors, and matrices are denoted by lowercase, boldface lowercase, and boldface uppercase letters, respectively. The Euclidean norm, statistical expectation, transpose, and the Hermitian transpose are represented by $\|\cdot\|_2$, $\mathbb{E}(\cdot)$, $(\cdot)^T$, and $(\cdot)^H$, respectively. The matrix $\mathbf{I}_N$ represents the $N \times N$ identity matrix. We denote the ith element of the vector $\mathbf{y}$ as $[\mathbf{y}]_i$ and the (i,j)th element of the matrix $\mathbf{Y}$ as $[\mathbf{Y}]_{i,j}$. The set of real-valued $M \times N$ matrices is denoted by $\mathbb{R}^{M\times N}$ and $\mathbb{R}^{M\times 1} = \mathbb{R}^M$. The cardinality of the set $\mathcal{A}$ is $|\mathcal{A}|$ and the ith element of the set is $\mathcal{A}(i)$. We use $\mathcal{N}(\mu,\sigma^2)$ or $\mathcal{CN}(\mu,\sigma^2)$, χ^2_d and $\chi'^2_d(\tau)$ to indicate the real or complex Gaussian distribution with mean μ and variance σ^2, the central chi-squared distribution with degrees of freedom d, and the non-central chi-squared distribution with the degrees of freedom d and the noncentrality parameter τ, respectively.

II. System Model

We consider an ambient system composed of an RF source, a single-antenna reader and a multi-antenna tag (Fig. 1). We assume that the tag is equipped with K ($K \geq 2$) antennas. These K antennas are divided into two sets: one set with M ($1 < M \leq K$) antennas is for backscattering, and the other set with $K - M$ antennas is for wireless energy harvesting. Thus, these two tasks occur simultaneously and independently. In other words, the RF signals received by energy-harvesting antennas are reserved purely for powering the circuit, while the RF signals received by the active backscatter antennas are entirely devoted to backscattering. We denote the whole candidate antenna set as $\mathcal{A} = \{1, 2, \ldots, K\}$ and the backscatter antenna set as $\mathcal{S} = \{\kappa_1, \kappa_2, \ldots, \kappa_M\}$, where $\mathcal{S} \subseteq \mathcal{A}$.

Let h denote the channel between the RF source and the reader. Let the channels from the antenna $\kappa_m \in \mathcal{S}$ of the tag to the RF source and the reader be f_{κ_m} and g_{κ_m}, where $1 \leq m \leq M$. Let the RF source transmit complex Gaussian random signal $x(n)$ with transmitted power P_s. The signal received at the antenna $\kappa_m \in \mathcal{S}$ is given by [10]

$$r_m(n) = f_{\kappa_m} x(n). \tag{1}$$

This antenna then backscatters the signal $r_m(n)$ and transmits its own binary signal B. Specifically, $B = 0$ indicates that the tag changes its impedance so that solely a relatively very small amount of the RF signal is reflected, and $B = 1$ implies that the tag switches the impedance so as to backscatter some of the RF signal. Consequently, the backscattered signal by the antenna $\kappa_m \in \mathcal{S}$ is

$$r_b^m(n) = \alpha B r_m(n), \tag{2}$$

where $\alpha \in [0, 1]$ represents the attenuation inside the tag, which is achieved by adjusting the load impedance at the port of the antenna, and also depends on the structure mode of the antenna [36], [37]. It determines the amount of the incident RF signals to be backscattered [38]. Finally, the received signal at the reader can be expressed as

$$\begin{aligned} y(n) &= hx(n) + g_{\kappa_m} r_b^m(n) + \omega(n) \\ &= \begin{cases} hx(n) + \omega(n), & B = 0, \\ (h + \alpha f_{\kappa_m} g_{\kappa_m}) x(n) + \omega(n), & B = 1, \end{cases} \end{aligned} \tag{3}$$

where $\omega(n) \sim \mathcal{CN}(0, \sigma_0^2)$ is additive white Gaussian noise (AWGN) at the reader.

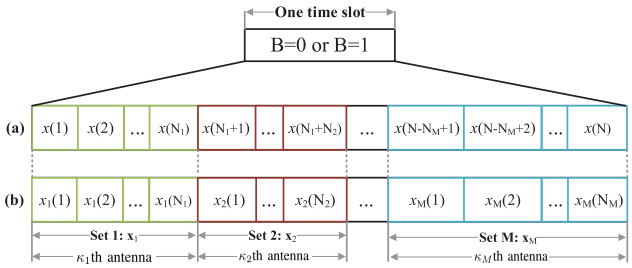

Fig. 2. GBS of the tag in one time slot: (a) N RF signals received by the tag, (b) backscattered signals by M backscatter antennas.

Because the data rate of the tag is much lower than that of the RF source, i.e., the tag signal B remains unchanged during N consecutive $x(n)$ in one time slot, we divide the N RF signals in one time slot into M sets, where the mth set contains an arbitrary number of signals N_m such that $\sum_{m=1}^{M} N_m = N$. As Fig. 2 shows, the mth set is given by

$$\mathbf{x}_m = [x_m(1), x_m(2), \ldots, x_m(N_m)]^T, \tag{4}$$

where $1 \leq m \leq M$.

When the tag receives the mth RF signal set, the mth backscatter antenna κ_m is active and reflects these RF signals; in other words, only one antenna is selected at one time for backscattering due to limited power. While the other $K - 1$ antennas are all connected to the energy harvester, and collect energy from both the RF signals and the backscattered signals of the antenna $\kappa_m \in \mathcal{S}$.[1]

According the references [40], [41], the energy harvesting efficiency depends on the value of load impedance in the matching network, which is connected to the multiple antennas to transfer maximum power from the antennas to the rectifier. As well, the rectifier is equipped with multiple diodes, which leads to nonlinear RF-to-DC conversion. Clearly, the energy harvester is then a nonlinear device.[2] The energy captured by both the $K - M$ antennas dedicated to wireless energy harvesting and the $M - 1$ silent backscatter antennas provides the power required for the backscatter communication with the antenna $\kappa_m \in \mathcal{S}$.

[1]The amount of harvested energy is typically on the order of micro-watts when the battery-free tags locate close to the RF source, such as TV tower with transmit power 10^6 W [42]. Thus, the harvested energy is sufficient for powering the analog components of the ambient backscatter devices, which consume 0.79 μW to 2 mW [2], [38].

[2]Since the energy harvester and the transmitter operate independently and simultaneously, the energy harvesting model has no effect on the backscattered signal (2) by the backscatter antennas, and the received signal at the reader (3). We only focus on the detector design in our work.

By defining the combined channel that corresponds to the mth backscatter as

$$\mu_{\kappa_m} = h + \alpha f_{\kappa_m} g_{\kappa_m}, \tag{5}$$

we further assume that all channels remain static for at least one time slot. The received signals at the reader from the antenna $\kappa_m \in \mathcal{S}$ can be written as

$$\mathbf{y}_m = \begin{cases} h\mathbf{x}_m + \boldsymbol{\omega}_m, & B = 0, \\ \mu_{\kappa_m}\mathbf{x}_m + \boldsymbol{\omega}_m, & B = 1, \end{cases} \tag{6}$$

where $\mathbf{y}_m = [y_m(1), y_m(2), \ldots, y_m(N_m)]^T$ and $\boldsymbol{\omega}_m = [\omega_m(1), \omega_m(2), \ldots, \omega_m(N_m)]^T$.

In one time slot, the signal detection problem is the following binary hypothesis testing

$$\begin{cases} \mathcal{H}_0 : \mathbf{y} = h\mathbf{x} + \boldsymbol{\omega}, & B = 0, \\ \mathcal{H}_1 : \mathbf{y} = \mathbf{F}\mathbf{x} + \boldsymbol{\omega}, & B = 1, \end{cases} \tag{7}$$

where $\mathbf{y} = [\mathbf{y}_1^T, \mathbf{y}_2^T, \cdots, \mathbf{y}_M^T]^T$, $\boldsymbol{\omega} = [\boldsymbol{\omega}_1^T, \boldsymbol{\omega}_2^T, \cdots, \boldsymbol{\omega}_M^T]^T$ and

$$\mathbf{F} = \mathrm{diag}[\underbrace{\mu_{\kappa_1}, \ldots, \mu_{\kappa_1}}_{N_1}, \underbrace{\mu_{\kappa_2}, \ldots, \mu_{\kappa_2}}_{N_2}, \ldots, \underbrace{\mu_{\kappa_M}, \ldots, \mu_{\kappa_M}}_{N_M}]. \tag{8}$$

The key issue of the ambient backscatter communications is for the reader to recover the tag signal B.

III. Detection Algorithm

As mentioned before, due to the limited power availability at the tag and few training symbols available from the tag, it is difficult for the reader to estimate the multiple channel parameters h and μ_{κ_m}. Moreover, the RF signal power P_s and the noise variance σ_0^2 are unknown at the reader, due to the uncontrollable nature of RF sources. Consequently, it is extremely important for the reader to be able to test the hypothesis (7) and to detect the tag signal without any knowledge these parameters. To this end, we develop a blind detector based on GLRT, which is a general approach for the hypothesis testing problem with unknown parameters. The fundamental principle of GLRT is to replace the unknown parameters with their MLEs and then compute the ratio of the probability density functions (PDFs) under $\mathcal{H}_0$ and $\mathcal{H}_1$ as the GLRT statistic.

It is readily found that the received signal in the mth set $y_m(n)$ has the following distributions

$$\begin{cases} \mathcal{H}_0 : y_m(n) \sim \mathcal{CN}\left(0, |h|^2 P_s + \sigma_0^2\right), & B = 0, \\ \mathcal{H}_1 : y_m(n) \sim \mathcal{CN}\left(0, |\mu_{\kappa_m}|^2 P_s + \sigma_0^2\right), & B = 1, \end{cases} \tag{9}$$

where $m = 1, 2, \ldots, M$ and $n = 1, 2, \ldots, N_m$. Then the received signals $\mathbf{y}$ (7) in one time slot have the distributions

$$\begin{cases} \mathcal{H}_0 : \mathbf{y} \sim \mathcal{CN}\left(\mathbf{0}, \mathbf{C}_0\right), & B = 0, \\ \mathcal{H}_1 : \mathbf{y} \sim \mathcal{CN}\left(\mathbf{0}, \mathbf{C}_1\right), & B = 1, \end{cases} \tag{10}$$

where the covariance matrices under $\mathcal{H}_0$ and $\mathcal{H}_1$ can be expressed as

$$\begin{aligned} \mathbf{C}_i &= \mathbb{E}\{(\mathbf{y} - \mathbb{E}\{\mathbf{y}\})(\mathbf{y} - \mathbb{E}\{\mathbf{y}\})^H\} \\ &= \begin{cases} (|h|^2 P_s + \sigma_0^2)\mathbf{I}_N, & i = 0, \\ \mathbf{F}\mathbf{F}^H P_s + \sigma_0^2 \mathbf{I}_N, & i = 1. \end{cases} \end{aligned} \tag{11}$$

Accordingly, the unknown parameter sets under $\mathcal{H}_0$ and $\mathcal{H}_1$ are given by

$$\Theta_0 = \{P_s, \sigma_0^2, h\}, \ \Theta_1 = \{P_s, \sigma_0^2, \mu_{\kappa_1}, \mu_{\kappa_2}, \ldots, \mu_{\kappa_M}\}. \tag{12}$$

By using GLRT, we obtain the MLEs of the unknown parameters under $\mathcal{H}_0$ and $\mathcal{H}_1$ as

$$\widehat{\Theta}_0 = \arg\max_{\Theta_0} p(\mathbf{y}; \Theta_0, \mathcal{H}_0), \ \widehat{\Theta}_1 = \arg\max_{\Theta_1} p(\mathbf{y}; \Theta_1, \mathcal{H}_1), \tag{13}$$

where the PDF of the received signals $\mathbf{y}$ under $\mathcal{H}_0$ and under $\mathcal{H}_1$ can be expressed as

$$\begin{aligned} p(\mathbf{y}; \Theta_0, \mathcal{H}_0) &= \frac{1}{\pi^N \det(\mathbf{C}_0)} \exp\left(-\mathbf{y}^H \mathbf{C}_0^{-1} \mathbf{y}\right) \\ &= \frac{1}{\pi^N (|h|^2 P_s + \sigma_0^2)^N} \exp\left(-\frac{\mathbf{y}^H \mathbf{y}}{|h|^2 P_s + \sigma_0^2}\right), \end{aligned} \tag{14}$$

and

$$\begin{aligned} p(\mathbf{y}; \Theta_1, \mathcal{H}_1) &= \frac{1}{\pi^N \det(\mathbf{C}_1)} \exp\left(-\mathbf{y}^H \mathbf{C}_1^{-1} \mathbf{y}\right) \\ &= \frac{1}{\pi^N \left(\prod_{m=1}^M (|\mu_{\kappa_m}|^2 P_s + \sigma_0^2)^{N_m}\right)} \\ &\quad \times \exp\left(-\sum_{m=1}^M \frac{\mathbf{y}_m^H \mathbf{y}_m}{|\mu_{\kappa_m}|^2 P_s + \sigma_0^2}\right), \end{aligned} \tag{15}$$

respectively. After replacing (12) with (13) and calculating the ratio of the PDFs under under $\mathcal{H}_0$ and $\mathcal{H}_1$, the general form of the GLRT statistic can be written as

$$T_{\mathrm{GLRT}} = \frac{p(\mathbf{y}; \widehat{\Theta}_1, \mathcal{H}_1)}{p(\mathbf{y}; \widehat{\Theta}_0, \mathcal{H}_0)}. \tag{16}$$

However, obtaining the MLEs of the parameters P_s, σ_0^2, h and μ_{κ_m} separately is difficult since they interact. To address this challenge, we next redefine the unknown parameter sets (12) as

$$\Theta_0 = \mathbf{C}_0, \ \Theta_1 = \mathbf{C}_1, \tag{17}$$

and directly derive the MLEs of $\mathbf{C}_0$ and $\mathbf{C}_1$ [47].

A. GLRT Based Detector Design With GBS

Since the unknown covariance matrix $\mathbf{C}_0$ only depends on the parameter $|h|^2 P_s + \sigma_0^2$, we first derive the MLE of the parameter $|h|^2 P_s + \sigma_0^2$ to construct the MLE of $\mathbf{C}_0$. For simplification, we define

$$\varepsilon = |h|^2 P_s + \sigma_0^2. \tag{18}$$

From (14), the log-likelihood function (LLF) under $\mathcal{H}_0$ is given by

$$\begin{aligned} \ln p(\mathbf{y}; \mathbf{C}_0, \mathcal{H}_0) &= -N \ln \pi - \ln\left(\det(\mathbf{C}_0)\right) - \mathbf{y}^H \mathbf{C}_0^{-1} \mathbf{y} \\ &= -N \ln \pi - N \ln \varepsilon - \frac{\mathbf{y}^H \mathbf{y}}{\varepsilon}. \end{aligned} \tag{19}$$

By setting the first derivative of the LLF (19) with respect to ε equal to zero, i.e.,

$$\frac{\partial \ln p(\mathbf{y}; \mathbf{C}_0, \mathcal{H}_0)}{\partial \varepsilon} = -N \frac{1}{\varepsilon} + \frac{\mathbf{y}^H \mathbf{y}}{\varepsilon^2} = 0, \tag{20}$$

the MLE $\hat{\varepsilon}$ is obtained as $\frac{\mathbf{y}^T\mathbf{y}}{N}$, and the MLE of $\mathbf{C}_0$ is

$$\widehat{\mathbf{C}}_0 = \hat{\varepsilon}\mathbf{I}_N = \frac{\mathbf{y}^H\mathbf{y}}{N}\mathbf{I}_N. \tag{21}$$

Next, to derive the MLE of the covariance matrix $\mathbf{C}_1$, we define $\mathbf{A} = \mathbf{C}_1^{-1}$. From (15), the LLF under $\mathcal{H}_1$ can be written as

$$\begin{aligned}
&\ln p(\mathbf{y}; \mathbf{C}_1, \mathcal{H}_1) \\
&\quad = -N\ln\pi - \ln\left(\det(\mathbf{C}_1)\right) - \mathbf{y}^H\mathbf{C}_1^{-1}\mathbf{y} \qquad (22)\\
&\quad = \underbrace{-N\ln\pi + \ln\left(\det(\mathbf{A})\right) - \mathbf{y}^H\mathbf{A}\mathbf{y}}_{\ln p(\mathbf{y};\mathbf{A},\mathcal{H}_1)}. \qquad (23)
\end{aligned}$$

Taking advantage of the fact that $\frac{\partial \ln(\det(\mathbf{A}))}{\partial \mathbf{A}} = \mathbf{A}^{-1}$, we have

$$\frac{\partial^2 \ln p(\mathbf{y}; \mathbf{A}, \mathcal{H}_1)}{\partial \mathbf{A}^2} = \frac{\partial^2 \ln\left(\det(\mathbf{A})\right)}{\partial \mathbf{A}^2} = -\mathbf{A}^{-2}. \tag{24}$$

Since $\mathbf{A}$ is positive semi-definite, the LLF (23) is a concave function of $\mathbf{A}$. The MLE of $\mathbf{A}$ can be obtained by setting the first derivative of the LLF (23) to the all-zero matrix, i.e.,

$$\frac{\partial \ln p(\mathbf{y}; \mathbf{A}, \mathcal{H}_1)}{\partial \mathbf{A}} = \mathbf{A}^{-1} - \mathbf{y}\mathbf{y}^T = \mathbf{0}. \tag{25}$$

Thus the MLE of $\mathbf{A}$ is $\left(\mathbf{y}\mathbf{y}^H\right)^{-1}$ and the MLE of $\mathbf{C}_1$ is

$$\widehat{\mathbf{C}}_1 = \widehat{\mathbf{A}}^{-1} = \mathbf{y}\mathbf{y}^H. \tag{26}$$

The GLRT statistic (16) for the scheme in Fig. 2 is further obtained as

$$T^g_{\mathrm{GLRT}} = \frac{p(\mathbf{y}; \widehat{\mathbf{C}}_1, \mathcal{H}_1)}{p(\mathbf{y}; \widehat{\mathbf{C}}_0, \mathcal{H}_0)}. \tag{27}$$

Unfortunately, the above GLRT statistic (27) fails to detect the tag signal, as will be shown in the following theorem.

Theorem 1: The GLRT statistic (27) when the GBS in Fig. 2 is used is not valid for the detection of the tag signal.

Proof: Substituting (21) and (26) into (19) and (22), respectively, we finally derive the log-GLRT statistic as

$$\begin{aligned}
T_g &= \ln T^g_{\mathrm{GLRT}} \\
&= \ln p(\mathbf{y}; \widehat{\mathbf{C}}_1, \mathcal{H}_1) - \ln p(\mathbf{y}; \widehat{\mathbf{C}}_0, \mathcal{H}_0) \\
&= \ln\left(\det(\widehat{\mathbf{C}}_0)\right) + \mathbf{y}^H\widehat{\mathbf{C}}_0^{-1}\mathbf{y} - \ln\left(\det(\widehat{\mathbf{C}}_1)\right) - \mathbf{y}^H\widehat{\mathbf{C}}_1^{-1}\mathbf{y} \\
&= N\ln\left(\frac{\mathbf{y}^H\mathbf{y}}{N}\right) + \mathbf{y}^H\left(\frac{\mathbf{y}^H\mathbf{y}}{N}\mathbf{I}_N\right)^{-1}\mathbf{y} \\
&\quad - \ln\left(\det(\widehat{\mathbf{C}}_1)\right) - \mathbf{y}^H(\mathbf{y}\mathbf{y}^H)^{-1}\mathbf{y} \\
&= N\ln\left(\frac{\mathbf{y}^H\mathbf{y}}{N}\right) + N - \ln\left(\det(\widehat{\mathbf{C}}_1)\right) \\
&\quad - \mathrm{tr}\left[(\mathbf{y}\mathbf{y}^H)(\mathbf{y}\mathbf{y}^H)^{-1}\right] \\
&= N\ln\left(\frac{\mathrm{tr}(\widehat{\mathbf{C}}_1)}{N}\right) - \ln\left(\det(\widehat{\mathbf{C}}_1)\right), \qquad (28)
\end{aligned}$$

where $\mathrm{tr}\left[(\mathbf{y}\mathbf{y}^H)(\mathbf{y}\mathbf{y}^H)^{-1}\right] = \mathrm{tr}(\mathbf{I}_N) = N$.

According to (26), the rank of the matrix $\widehat{\mathbf{C}}_1$ is equal to one, which indicates the determinant of the matrix $\widehat{\mathbf{C}}_1$ is equal to zero and the log-GLRT statistic (28) is not valid. As a result, the GLRT-based algorithm proposed in [47] can not be directly applied to our ambient backscatter communication systems. ■

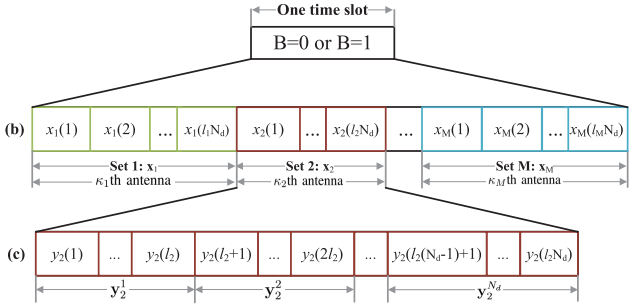

Fig. 3. SDBS of the tag in one time slot: (b) a quantized number of RF signals per backscatter antenna, (c) the division of the mth received signal set at the reader.

Remark 1: An alternative estimation of covariance matrix $\mathbf{C}_1$ (11) is to estimate the diagonal elements of $\mathbf{C}_1$ separately and then assemble a new diagonal matrix. However, to derive the required values, the tag needs to insert at least 1 bit identifier before the backscattered signals of each antenna, which costs extra energy and reduces the data rate of the tag. In addition, estimating the entire matrix $\mathbf{C}_1$ as (26), which contains all uncertain diagonal values, may reduce the computational complexity.

B. GLRT Based Detector Design With SDBS

We have shown that GLRT fails when using GBS in Fig. 2. To overcome this drawback, we present a new backscatter scheme for the tag in Fig. 3, where the number of sequential backscattered signals in each set N_m is a multiple of N_d ($N_d > 1$), i.e., $N_m = l_m N_d$. We further assume that l_m and the common divisor N_d are positive integers, which satisfy the conditions $N_d \sum_{m=1}^{M} l_m = N$ and $\sum_{m=1}^{M} l_m = L$.

As Fig. 3 shows, the RF signals in the mth set (4) and the received signals at the reader in the mth set (6) can be further expressed as $\mathbf{x}_m = [x_m(1), x_m(2), \ldots, x_m(l_m N_d)]^T$ and

$$\mathbf{y}_m = [y_m(1), y_m(2), \ldots, y_m(l_m N_d)]^T, \tag{29}$$

respectively, where $1 \le m \le M$. Then we reclassify the mth received signal set $\mathbf{y}_m$ (29) into N_d groups and each group is given by

$$\mathbf{y}_m^n = [y_m\left(l_m(n-1)+1\right), \ldots, y_m(l_m n)]^T, \tag{30}$$

where $1 \le n \le N_d$. Therefore, there exist MN_d groups. N_d can be roughly thought of as the sample size in the process of the estimation of correlation matrices. Using the MN_d groups, we reconstruct the received signals $\mathbf{y}$ into N_d observation sets as

$$\begin{aligned}
\tilde{\mathbf{y}}_n &= [(\mathbf{y}_1^n)^T, (\mathbf{y}_2^n)^T, \ldots, (\mathbf{y}_M^n)^T]^T \\
&= [y_1\left(l_1(n-1)+1\right), \ldots, y_1(l_1 n), y_2\left(l_2(n-1)+1\right), \\
&\quad \ldots, y_2(l_2 n), \ldots, y_M\left(l_M(n-1)+1\right), \ldots, y_M(l_M n)]^T. \qquad (31)
\end{aligned}$$

Similarly to (11), the covariance matrix of nth observation set under $\mathcal{H}_1$ can be computed as

$$\begin{aligned}
\mathbf{C}_1^n &= \mathbb{E}\{(\tilde{\mathbf{y}}_n - \mathbb{E}\{\tilde{\mathbf{y}}_n\})(\tilde{\mathbf{y}}_n - \mathbb{E}\{\tilde{\mathbf{y}}_n\})^H\} \\
&= \mathrm{diag}\{\underbrace{\sigma_1^2, \ldots, \sigma_1^2}_{l_1}, \underbrace{\sigma_2^2, \ldots, \sigma_2^2}_{l_2}, \ldots, \underbrace{\sigma_M^2, \ldots, \sigma_M^2}_{l_M}\}, \qquad (32)
\end{aligned}$$

where

$$\sigma_m^2 = |\mu_{\kappa_m}|^2 P_s + \sigma_0^2. \tag{33}$$

By defining $\tilde{\mathbf{C}}_1 = \mathbf{C}_1^n$, it can be readily checked that the covariance matrices of the N_d observation sets under $\mathcal{H}_1$ are identical, i.e., $\mathbf{C}_1^1 = \mathbf{C}_1^2 = \ldots = \mathbf{C}_1^{N_d} = \tilde{\mathbf{C}}_1$.

Accordingly, the LLF under $\mathcal{H}_1$ (22) can be rewritten as

$$\begin{aligned}
&\ln p(\mathbf{y}; \mathbf{C}_1, \mathcal{H}_1) \\
&= -N \ln \pi \\
&\quad -N_d \ln \left(\prod_{m=1}^{M} (|\mu_{\kappa_m}|^2 P_s + \sigma_0^2)^{l_m} \right) - \sum_{m=1}^{M} \frac{\mathbf{y}_m^H \mathbf{y}_m}{|\mu_{\kappa_m}|^2 P_s + \sigma_0^2} \\
&= -N \ln \pi - N_d \ln \left(\det(\tilde{\mathbf{C}}_1) \right) - \sum_{n=1}^{N_d} \tilde{\mathbf{y}}_n^H \tilde{\mathbf{C}}_1^{-1} \tilde{\mathbf{y}}_n.
\end{aligned} \tag{34}$$

Instead of computing the MLE of $\mathbf{C}_1$ as (26), we obtain the MLE of $\tilde{\mathbf{C}}_1$ utilizing the N_d observation sets. Similar to the calculation of the MLE of $\mathbf{C}_1$, we denote $\tilde{\mathbf{C}}_1^{-1}$ as $\tilde{\mathbf{A}}$ and rewrite the LLF under $\mathcal{H}_1$ (34) as

$$\begin{aligned}
&\ln p(\mathbf{y}; \mathbf{C}_1, \mathcal{H}_1) \\
&\quad = \underbrace{-N \ln \pi + N_d \ln \left(\det(\tilde{\mathbf{A}}) \right) - \sum_{n=1}^{N_d} \tilde{\mathbf{y}}_n^H \tilde{\mathbf{A}} \tilde{\mathbf{y}}_n}_{\ln p(\mathbf{y}; \tilde{\mathbf{A}}, \mathcal{H}_1)}.
\end{aligned} \tag{35}$$

Noting that $\tilde{\mathbf{A}}$ is positive semi-definite and $\frac{\partial^2 \ln p(\mathbf{y}; \tilde{\mathbf{A}}, \mathcal{H}_1)}{\partial \tilde{\mathbf{A}}^2} = -\tilde{\mathbf{A}}^{-2}$, thus the LLF (35) is a concave function. By setting the first derivative of the LLF (35) to the all-zero matrix, the MLE of $\tilde{\mathbf{A}}$ is derived as $\left(\frac{1}{N_d} \sum_{n=1}^{N_d} \tilde{\mathbf{y}}_n \tilde{\mathbf{y}}_n^H \right)^{-1}$ and the MLE of $\tilde{\mathbf{C}}_1$ is given by

$$\hat{\tilde{\mathbf{C}}}_1 = \frac{1}{N_d} \sum_{n=1}^{N_d} \tilde{\mathbf{y}}_n \tilde{\mathbf{y}}_n^H. \tag{36}$$

Clearly, larger values of N_d lead us to better estimates.

Unlike the estimated matrix $\widehat{\mathbf{C}}_1$ (26) with rank one in subsection III-A, which leads to an invalid GLRT statistic (28), the estimated matrix $\hat{\tilde{\mathbf{C}}}_1$ is of full rank, which facilitates the derivation of an efficient GLRT statistic as

$$T_{\mathrm{GLRT}}^s = \frac{p(\mathbf{y}; \hat{\tilde{\mathbf{C}}}_1, \mathcal{H}_1)}{p(\mathbf{y}; \widehat{\mathbf{C}}_0, \mathcal{H}_0)}. \tag{37}$$

Theorem 2: Let $\tilde{\lambda}_1, \tilde{\lambda}_2, \ldots, \tilde{\lambda}_L$ denote the eigenvalues of $\hat{\tilde{\mathbf{C}}}_1$. The decision statistic (37) of the GLRT based detector using SDBS in Fig. 3 can be expressed as

$$T_{s1} = \frac{\frac{1}{L} \sum_{l=1}^{L} \tilde{\lambda}_l}{\left(\prod_{l=1}^{L} \tilde{\lambda}_l \right)^{\frac{1}{L}}}. \tag{38}$$

Proof: The log-GLRT statistic can be written as

$$\begin{aligned}
T_s &= \ln T_{\mathrm{GLRT}}^s = \ln p(\mathbf{y}; \hat{\tilde{\mathbf{C}}}_1, \mathcal{H}_1) - \ln p(\mathbf{y}; \widehat{\mathbf{C}}_0, \mathcal{H}_0) \qquad (39) \\
&= -N_d \ln \left(\det(\hat{\tilde{\mathbf{C}}}_1) \right) - \sum_{n=1}^{N_d} \tilde{\mathbf{y}}_n^H \hat{\tilde{\mathbf{C}}}_1^{-1} \tilde{\mathbf{y}}_n \\
&\quad + \ln \left(\det(\widehat{\mathbf{C}}_0) \right) + \mathbf{y}^H \widehat{\mathbf{C}}_0^{-1} \mathbf{y}. \qquad (40)
\end{aligned}$$

Substituting (21) and (36) into (19) and (34), respectively, the log-GLRT statistic can be further derived as

$$\begin{aligned}
T_s &= -N_d \ln \left(\det(\hat{\tilde{\mathbf{C}}}_1) \right) - N_d \sum_{n=1}^{N_d} \tilde{\mathbf{y}}_n^H \left(\sum_{n=1}^{N_d} \tilde{\mathbf{y}}_n \tilde{\mathbf{y}}_n^H \right)^{-1} \tilde{\mathbf{y}}_n \\
&\quad + N \ln \left(\frac{\mathbf{y}^H \mathbf{y}}{N} \right) + \mathbf{y}^H \left(\frac{\mathbf{y}\mathbf{y}^H}{N} \right)^{-1} \mathbf{y} \\
&= -N_d \ln \left(\det(\hat{\tilde{\mathbf{C}}}_1) \right) \\
&\quad - N_d \mathrm{tr} \left[\left(\sum_{n=1}^{N_d} \tilde{\mathbf{y}}_n \tilde{\mathbf{y}}_n^H \right) \left(\sum_{n=1}^{N_d} \tilde{\mathbf{y}}_n \tilde{\mathbf{y}}_n^H \right)^{-1} \right] \\
&\quad + N \ln \left(\frac{\mathbf{y}^H \mathbf{y}}{N} \right) + N \\
&= -N_d \ln \left(\det(\hat{\tilde{\mathbf{C}}}_1) \right) + N \ln \left(\frac{N_d \mathrm{tr}(\hat{\tilde{\mathbf{C}}}_1)}{N} \right),
\end{aligned} \tag{41}$$

where $N_d \mathrm{tr} \left[\left(\sum_{n=1}^{N_d} \tilde{\mathbf{y}}_n \tilde{\mathbf{y}}_n^H \right) \left(\sum_{n=1}^{N_d} \tilde{\mathbf{y}}_n \tilde{\mathbf{y}}_n^H \right)^{-1} \right] = N_d \mathrm{tr}(\mathbf{I}_L) = N$ and $\mathbf{y}^H \mathbf{y} = N_d \mathrm{tr}(\hat{\tilde{\mathbf{C}}}_1)$.

Utilizing the eigenvalues of the estimated covariance matrix $\hat{\tilde{\mathbf{C}}}_1$, we have

$$\det(\hat{\tilde{\mathbf{C}}}_1) = \prod_{l=1}^{L} \tilde{\lambda}_l, \ \mathrm{tr}\{\hat{\tilde{\mathbf{C}}}_1\} = \sum_{l=1}^{L} \tilde{\lambda}_l. \tag{42}$$

The log-GLRT statistic (41) can be rewritten as

$$\begin{aligned}
T_s &= -N_d \ln \left(\prod_{l=1}^{L} \tilde{\lambda}_l \right) + N \ln \left(\frac{N_d \sum_{l=1}^{L} \tilde{\lambda}_l}{N} \right) \\
&= -N \ln \left(\prod_{l=1}^{L} \tilde{\lambda}_l \right)^{\frac{1}{L}} + N \ln \left(\frac{\sum_{l=1}^{L} \tilde{\lambda}_l}{L} \right).
\end{aligned} \tag{43}$$

The decision statistic (38) is obtained by defining T_{s1} as $\exp\left(\frac{T_s}{N}\right)$. ■

It is observed that the distribution of the decision statistic T_{s1} (or the log-GLRT statistic T_s) is necessary for determining the decision threshold and constructing the decision rule to judge if the tag signal is bit '0' or bit '1'.

Theorem 3: The asymptotic distribution of the log-GLRT statistic T_s (39) is

$$2T_s \sim \begin{cases} \chi_{L^2}^2, & \text{under } \mathcal{H}_0, \\ \chi_{L^2}'^2(\tau), & \text{under } \mathcal{H}_1, \end{cases} \tag{44}$$

where τ is the noncentrality parameter of the non-central chi-squared distribution $\chi_{L^2}'^2(\tau)$ and can be expressed as

$$\tau = \frac{N}{\varepsilon^2 L^2} \sum_{m=1}^{M} l_m \delta_m^2. \tag{45}$$

Proof: See Appendix A. ■

Next, based on the distribution of the log-GLRT statistic T_s, we will obtain the decision threshold γ, determine the decision rule and further derive the performance measure in terms of detection probability.

Theorem 4: The decision rule of GLRT with SDBS in Fig. 3 can be described by

$$T_{s1} \underset{\mathcal{H}_0}{\overset{\mathcal{H}_1}{\gtrless}} \gamma, \tag{46}$$

where the threshold γ is obtained from a given false alarm probability P_{FA} and is given by

$$\gamma = \exp\left[\frac{1}{2N} Q^{-1}_{\chi^2_{L^2}}\left(P_{\mathrm{FA}}\right)\right]. \tag{47}$$

Thus, the detection probability can be derived as

$$P_D = Q_t\left(a, b\right), \tag{48}$$

where $a = \sqrt{\tau}$, $b = \sqrt{2N \ln \gamma}$, $t = \frac{L^2}{2}$, and $Q_t(a, b)$ represents the generalized Marcum-Q function [49].

Proof: From (44), the false alarm probability P_{FA} is computed by

$$\begin{aligned} P_{\mathrm{FA}} &= \Pr\{T_{s1} > \gamma; \mathcal{H}_0\} = \Pr\{2T_s > 2N \ln \gamma; \mathcal{H}_0\} \\ &= \int_{2N \ln \gamma}^{\infty} p(2T_s; \mathcal{H}_0) \mathrm{d}(2T_s) = Q_{\chi^2_{L^2}}(2N \ln \gamma), \end{aligned} \tag{49}$$

where $Q_{\chi^2_{L^2}}(\cdot)$ denotes the tail probability of the chi-squared distribution of degrees of freedom L^2 [46]. Given a fixed false alarm probability P_{FA}, the threshold γ (47) can be obtained after some straightforward computation.

The detection probability is calculated by

$$\begin{aligned} P_D &= \Pr\{T_{s1} > \gamma; \mathcal{H}_1\} \\ &= \Pr\{2T_s > 2N \ln \gamma; \mathcal{H}_1\} \int_{2N \ln \gamma}^{\infty} p(2T_s; \mathcal{H}_1) \mathrm{d}(2T_s) \\ &= \int_{2N \ln \gamma}^{\infty} \frac{1}{2} \left(\frac{2T_s}{\tau}\right)^{\frac{L^2-2}{4}} \\ &\quad \times \exp\left[-\frac{2T_s + \tau}{2}\right] I_{\frac{L^2}{2}-1}(\sqrt{2T_s \tau}) \mathrm{d}(2T_s), \end{aligned} \tag{50}$$

where $I_{\frac{L^2}{2}-1}(\cdot)$ is the modified Bessel function of order $\frac{L^2}{2} - 1$. By defining $x = \sqrt{2T_s}$, a, b and t, the detection probability (50) can be further expressed as

$$P_D = \int_b^{\infty} x \left(\frac{x}{a}\right)^{t-1} \exp\left(-\frac{x^2 + a^2}{2}\right) I_{t-1}(ax) \mathrm{d}x, \tag{51}$$

and finally reduced to (48). ∎

Proposition 1: The proposed GLRT based detector fails to find sufficient statistic when $K \geq M = 1$. Therefore, the GLRT based detector only works when at least two antennas are selected, i.e., $K \geq M \geq 2$.

Proof: See Appendix B. ∎

C. Modified Energy Detector When P_s, σ_0^2 and h Are Known

For comparison, we present a modified energy detector here under the condition that the reader knows the RF signal power P_s, the noise variance σ_0^2, and the CSI between the RF source and the reader h.

Classical energy detector (see [50] and references therein) computes the average power of the received signals $\mathbf{y}$ and compare it with a threshold so as to decode the tag signal B [2]. For example, if the average power is larger than the threshold, we decide $B = 1$, on the contrary, we decide $B = 0$. However, in our system, the multiple channel parameters μ_{κ_m} as well as the size relationship among the channel parameters h and $\mu_{\kappa_m} (1 \leq m \leq M)$, are uncertain. Hence, the size relationship between the average power of the received signals in *reflecting* state and *non-reflecting* state is not clear. Given the threshold, it is obscure to judge $B = 0$ or $B = 1$ when the the average power of the received signals is greater than the threshold.

To this end, we extend the classical energy detector to the proposed multi-antenna case through computing the sample variance of the received signals $\mathbf{y}$ as $\frac{\|\mathbf{y}\|_2^2}{N}$ and comparing it with a known specified value $\frac{|h|^2 P_s + \sigma_0^2}{2}$. From (10), it can be found that the ratio $\frac{2\|\mathbf{y}\|_2^2}{N(|h|^2 P_s + \sigma_0^2)}$ approximates to 1 under $\mathcal{H}_0$, but may be either close to 0 or larger than 1 under $\mathcal{H}_1$. Based on this observation, we define the decision statistic for the modified energy detector as $T_e = \frac{2\|\mathbf{y}\|_2^2}{|h|^2 P_s + \sigma_0^2}$, which is a chi-squared random variable with $2N$ degrees of freedom when the tag signal is $B = 0$. Subsequently, we perform the binary hypothesis test problem (7) utilizing the two-tail chi-squared test [15], [51]

$$\begin{cases} \text{decide } \mathcal{H}_0, & \text{if } \gamma_l \leq T_e \leq \gamma_r, \\ \text{decide } \mathcal{H}_1, & \text{if } T_e < \gamma_l \text{ or } T_e > \gamma_r, \end{cases} \tag{52}$$

where the left threshold γ_l and the right threshold γ_r related to the given false alarm probability P_{FA} are given as

$$\gamma_l = Q^{-1}_{\chi^2_{2N}}\left(1 - \frac{P_{\mathrm{FA}}}{2}\right), \ \gamma_r = Q^{-1}_{\chi^2_{2N}}\left(\frac{P_{\mathrm{FA}}}{2}\right). \tag{53}$$

IV. Optimal Backscatter Antenna Selection

To reduce the cost and the computational complexity, battery-free tags are physically small and eliminate power-hungry components, such as oscillators and filters, which are commonly used to detect signals or estimate the channels. For such battery-free devices, two to four separated antennas are commercially feasible, according to [35]. Let $\mathcal{A} = \{1, 2, \ldots, K\}$ denote the whole antenna set and $\mathcal{S} = \{\kappa_1, \kappa_2, \ldots, \kappa_M\}$ denote the candidate backscatter antenna set. We set the number of antennas as $K \in [2, 4]$ and the number of selected antennas as $M \in [2, 4]$. Without loss of generality, we assume that the combined channel modulus that correspond to $\mathcal{A}$ and $\mathcal{S}$ are ordered as

$$|\mu_1| \geq |\mu_2| \geq \ldots \geq |\mu_K|, \tag{54}$$

and

$$|\mu_{\kappa_1}| \geq |\mu_{\kappa_2}| \geq \ldots \geq |\mu_{\kappa_M}|, \tag{55}$$

respectively. It can be easily found from (33) and (55) that

$$\sigma_1^2 > \sigma_2^2 > \ldots > \sigma_M^2 > 0. \tag{56}$$

This section investigates how to select the optimal backscatter antennas, i.e., $\mathcal{S}_{opt}$, from the whole candidate antenna set $\mathcal{A}$ so as to maximize the detection probability P_D at the reader. Note that the probability of detection is defined as the probability that the GLRT based detector decides $\mathcal{H}_1$ by using the decision rule in (46) when the tag transmits '1' bit. Thus, given

the decision threshold γ (47), to maximize the probability of deciding $\mathcal{H}_1$, i.e., the probability that the decision statistic T_{s1} (38) is greater than the decision threshold γ, we maximize the decision statistic T_{s1}.

Next, in order to help with the analysis of the optimal backscatter antenna selection scheme, we transform the decision statistic T_{s1} (38) composed of the eigenvalues of the estimated covariance matrix $\widehat{\tilde{\mathbf{C}}}_1$ (36) to that composed of the diagonal elements of the covariance matrix $\tilde{\mathbf{C}}_1$ (32), which is stated in the following theorem.

Theorem 5: As the number of RF signals N goes to infinity, the decision statistic T_{s1} (38) can be further expressed as

$$T_{s1} = \frac{\frac{1}{L}\sum_{m=1}^{M} l_m \sigma_m^2}{\left(\prod_{m=1}^{M} (\sigma_m^2)^{l_m}\right)^{\frac{1}{L}}}. \tag{57}$$

Proof: The decision statistic T_{s1} is the ratio of the arithmetic mean to the geometric mean of the eigenvalues $\{\tilde{\lambda}_1, \tilde{\lambda}_2, \ldots, \tilde{\lambda}_L\}$. As $N \to \infty$, we have $\widehat{\tilde{\mathbf{C}}}_1 = \tilde{\mathbf{C}}_1$, i.e.,

$$\tilde{\lambda}_{\sum_{i=0}^{m-1} l_m+1} = \tilde{\lambda}_{\sum_{i=0}^{m-1} l_m+2} = \ldots = \tilde{\lambda}_{\sum_{i=0}^{m} l_m} = \sigma_m^2, \tag{58}$$

where $l_0 = 0$. Hence, by replacing the eigenvalues with σ_m^2, where $1 \le m \le M$, the decision statistic T_{s1} (38) is simplified to (57). ∎

Since the number of candidate antennas is sets as $K \in [2, 4]$ in our work, all candidate antennas are regarded as backscatter antenna when $M = K = 4$. Therefore, we will only consider the case of $M < K$ next and present the optimal backscatter antenna selection scheme for the cases of $M = 2$ and $M = 3$, respectively.

Proposition 2: In the case of $M = 2$, to maximize the GLRT statistic, the antennas with the largest channel modulus $|\mu_1|$ and the smallest channel modulus $|\mu_K|$ should be selected, i.e., the optimal antenna set is $\mathcal{S}_{opt} = \{1, K\}$.

Proof: When $M = 2$, i.e., the candidate backscatter antenna set is $\mathcal{S} = \{\kappa_1, \kappa_2\}$, it can be easily found from (56) that $\sigma_1^2 > \sigma_2^2$. Suppose the log-GLRT statistic T_{s1} (57) is a function of σ_1^2. By taking derivative of T_{s1} (57) with respect to σ_1^2, we have

$$\frac{\partial T_{s1}}{\partial \sigma_1^2} = \frac{l_1}{L}\left[(\sigma_1^2)^{l_1}(\sigma_2^2)^{l_2}\right]^{-\frac{1}{L}}\left(1 - \frac{l_1\sigma_1^2 + l_2\sigma_2^2}{L\sigma_1^2}\right). \tag{59}$$

Since $l_1\sigma_1^2 + l_2\sigma_2^2 < L\sigma_1^2$, the above first derivative is greater than zero and thus the statistic T_{s1} is a monotonous increasing function of σ_1^2. According to (33), the statistic T_{s1} is also strictly increasing with respect to $|\mu_{\kappa_1}|^2$.

Similarly, calculating the first derivative of the statistic T_{s1} (57) with respect to σ_2^2 gives

$$\frac{\partial T_{s1}}{\partial \sigma_2^2} = \frac{l_2}{L}\left[(\sigma_1^2)^{l_1}(\sigma_2^2)^{l_2}\right]^{-\frac{1}{L}}\left(1 - \frac{l_1\sigma_1^2 + l_2\sigma_2^2}{L\sigma_2^2}\right). \tag{60}$$

Since $l_1\sigma_1^2 + l_2\sigma_2^2 > L\sigma_2^2$, the first derivative (60) is smaller than zero and thus the statistic T_{s1} is a monotonous decreasing function of σ_2^2, as well as $|\mu_{\kappa_2}|^2$.

Therefore, to maximize the statistic T_{s1}, we maximize the variance $|\mu_{\kappa_1}|^2$ and minimize $|\mu_{\kappa_2}|^2$. According to (54), the antennas with the largest channel modulus $|\mu_1|$ and the smallest channel modulus $|\mu_K|$ should be selected. Therefore, the optimal antenna set is $\mathcal{S}_{opt} = \{1, K\}$. ∎

Algorithm 1 Optimal Backscatter Antenna Selection in the Case of $M = 3$

Input: Candidate antenna set $\mathcal{A} = \{1, 2, \ldots, K\}$; corresponding CSI $\mu_k, k = 1, 2, \ldots, K$; positive integers l_1, l_2, l_3;
Output: The optimal selected antenna set $\mathcal{S}_{opt} = \{\kappa_1, \kappa_2, \ldots, \kappa_M\}$
1: $\kappa_1 = 1$; $\kappa_M = K$;
2: **if** $l_1 > l_3$ **then** $\kappa_2 = K - 1$;
3: **else if** $l_1 < l_3$ **then** $\kappa_2 = 2$;
4: **else if** $|\mu_{\kappa_1}|^2 - |\mu_2|^2 < |\mu_{K-1}|^2 - |\mu_{\kappa_M}|^2$ **then** $\kappa_2 = 2$;
5: **else** $\kappa_2 = K - 1$;
6: **end if**
7: **return** $\mathcal{S}_{opt} = \{\kappa_1, \kappa_2, \kappa_3\}$

Proposition 3: In the case of $M = 3$, the optimal backscatter antenna set that can maximize the detection probability P_D is given by $\mathcal{S}_{opt} = \{1, \kappa_2, K\}$, where $\kappa_2 = 2$ or $\kappa_2 = K - 1$. Specifically, we summarize the optimal antenna selection scheme in Algorithm 1.

Proof: See Appendix C. ∎

Proposition 4: Among the two considered backscatter antenna sets, i.e., $M \in [2, 3]$, the set with the two antennas, which corresponds to $M = 2$ and consists of the antennas with the largest channel modulus and the smallest channel modulus, can provide the maximum detection performance at the reader.

Proof: See Appendix D. ∎

Remark 2: In order to obtain the size relationship of the channel modulus (54), the tag first divides N RF signals in one time slot into K sets. Then the kth ($1 \le k \le K$) antenna reflects the RF signals in kth RF signal set, i.e., the tag transmits '1' bit as a pilot symbol. After signal reception in one time slot, the reader obtains the size relationship of the combined channel modulus rather than the exact value of each combined channel by calculating the average energy of the K received signal sets. By using the estimated channel modulus, the reader determines the backscatter antennas via *Proposition* 2 and Algorithm 1. Finally, the selection result is transmitted to the tag.

Remark 3: We refer to a complex multiplier, adder (CMA) and a comparator as the basic computational complexity units (BCCU) at the reader. In order to derive the channel modulus by computing the average energy, the reader needs KN CMAs for the energy calculation. For the battery-free tag, it requires an envelope detection and averaging analog circuit, and a comparator to recover the information about the backscatter antennas transmitted by the reader.

V. Simulation Results

In this section, we examine the detection performance of the proposed GLRT based detector. We assume the AWGN term of $\mathcal{CN}(0, 1)$. The channel parameters h, f_k and g_k are generated as independent and identically distributed $\mathcal{CN}(0, 1)$, equivalently Rayleigh fading. We define the false alarm probability P_{FA} as 5%. Unless otherwise mentioned, we set $\alpha = 0.8$,

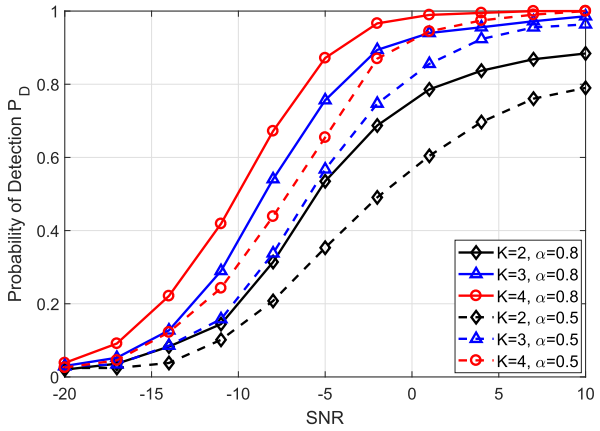

Fig. 4. P_D versus SNR for different number of candidate antennas K and different tag attenuation α.

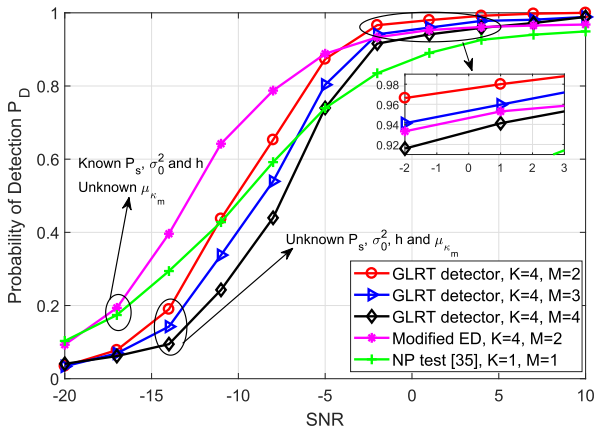

Fig. 5. P_D versus SNR for different number of backscatter antennas M.

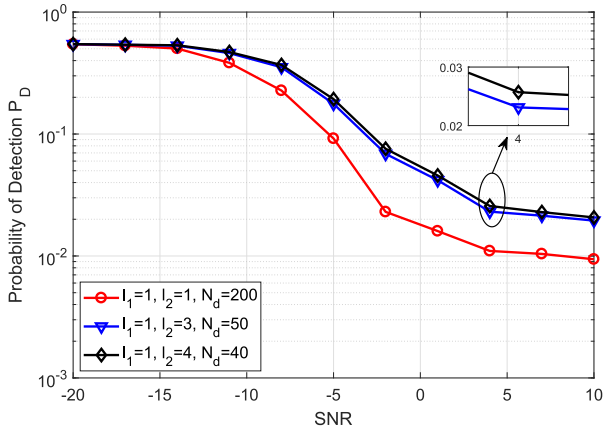

Fig. 6. BER versus SNR for different common divisor in SDBS N_d.

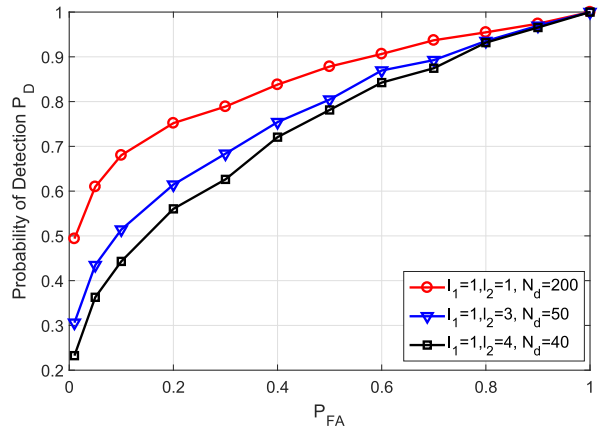

Fig. 7. P_D versus $P_{\rm FA}$ for different common divisor in SDBS N_d.

$l_k = 1$ ($k = 1, \ldots, M$), and use the optimal backscatter antenna selection scheme (Section IV).

In Fig. 4, the detection probabilities of the proposed detector are plotted against SNR for several values of the number of candidate antennas K. The curves have been depicted for two cases of $\alpha = 0.8$ and $\alpha = 0.5$. The numbers of backscatter antennas and RF signals are $M = 2$ and $N = 400$, respectively. Fig. 4 shows a clear improvement of detection probability for more candidate antennas. The reason is that multiple antennas at the tag provide the diversity gain [34], which contributes to better detection performance. Additionally, we see that lower tag attenuation degrades the detection performance of the proposed detector. The reason is that lower tag attenuation results in weaker backscatter signals.

An important question is the effect of the number of backscatter antennas (M) on the proposed detector (46). To answer this question, Fig. 5 plots the detection probability of (46) versus SNR for several values of M. The numbers of candidate antennas and RF signals are $K = 4$ and $N = 400$, respectively. Fig. 5 shows that the detector performs best when selecting only two backscatter antennas ($M = 2$), which corroborates *Proposition* 4. The reason is because GLRT compares the PDF under $\mathcal{H}_0$ (14) and the PDF under $\mathcal{H}_1$ (15), which is related with the covariance matrices (11). The covariance matrix under $\mathcal{H}_1$ depends on the channel modulus of the selected antennas. Choosing the two antennas with the largest channel modulus and the smallest channel modulus can maximize the difference between the two PDFs. For comparison, the detection probability of the modified energy detector (52) when $M = 2$ and that of the Neyman-Pearson (NP) test [46] when $K = 1$ are also plotted respectively. As expected, the modified energy detector outperforms the GLRT detector (46) when SNR is below -2 dB, since the former assumes perfect knowledge of the RF signal power, the noise variance and the CSI between the RF source and the reader. However, when SNR exceeds -2 dB, the proposed GLRT based detector outperforms the modified energy detector. We also observe that even the proposed GLRT based detector (with $M = 4$) outperforms the NP test with single-antenna tag when SNR exceeds -5 dB.

Fig. 6 indicates the bit error rate (BER) versus SNR for the backscatter schemes given in Fig. 3. For simplicity, we choose two optimal backscatter antennas and set the coefficient for the first set l_1 as 1. The common divisor N_d is set as 200, 50, and 40, respectively. Other parameters are set the same as those in Fig. 5. We observe that a larger value of N_d leads to a lower BER. The reason is that the MLE of the covariance matrix $\widehat{\tilde{\mathbf{C}}}_1$ (36) is more accurate when the value of N_d increases. This is also clear from Fig. 7 where the detection performance in terms of false alarm probability $P_{\rm FA}$ has been depicted. As we can see, the GLRT based detector achieves higher detection probability for larger N_d. Moreover, it can be also seen from Fig. 6 that the BER will approach an error floor when SNR reaches infinity [11].

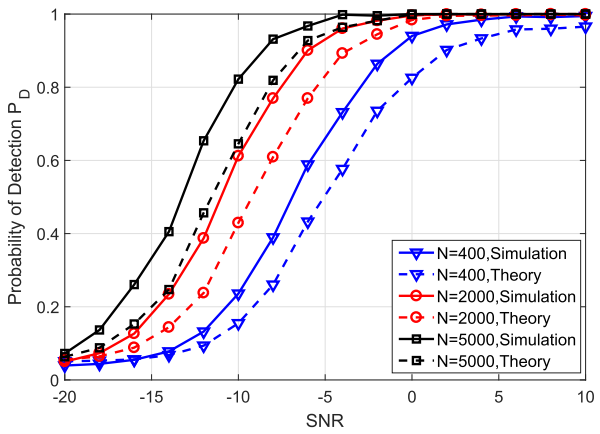

Fig. 8. Comparison between the asymptotic detection probabilities and the simulated results.

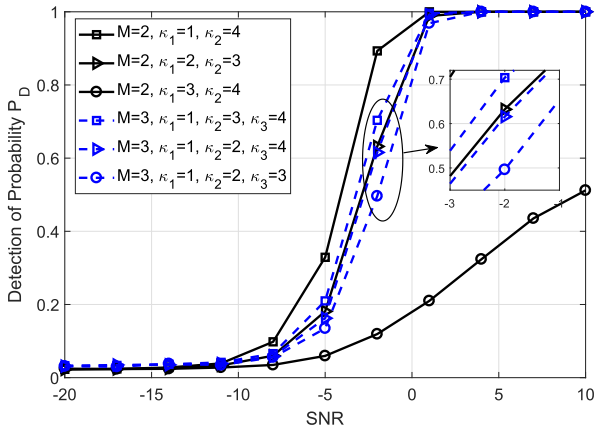

Fig. 9. P_D versus SNR for different backscatter antenna sets.

The asymptotic detection probabilities and the simulated results for different numbers of RF signals N are compared in Fig. 8. Here, we set the number of the RF signals in one time slot as 400, 2000, and 5000, respectively, since the approximate distribution is obtained when $N \to \infty$. Notable trends in this figure can be explained via the central limit theorem [52]. That is, when the value of N is extremely large, the MLEs $\widehat{\mathbf{C}}_0$ and $\widehat{\tilde{\mathbf{C}}}_1$ approximate the covariance matrices $\mathbf{C}_0$ and $\tilde{\mathbf{C}}_1$, respectively. As a result, the detection probability trends upward when the number of RF signals increases.

Finally, we investigate the optimal backscatter antenna selection scheme proposed in Section IV. We assume that the number of RF signals is $N = 300$ and the whole candidate antenna set includes six antennas, i.e., $K = 4$, while the corresponding channel modulus are $|\mu_1| = 1$, $|\mu_2| = 0.9$, $|\mu_3| = 0.3$, and $|\mu_4| = 0.2$, respectively. We focus on the detection probability for two cases, namely, $M = 2$ and $M = 3$. When $M = 2$, three candidate backscatter antenna sets are investigated: $\{1, 4\}$, $\{2, 3\}$, and $\{3, 4\}$. For the case of $M = 3$, we also consider three candidate backscatter antenna sets: $\{1, 3, 4\}$, $\{1, 2, 4\}$, and $\{1, 2, 3\}$. Fig. 9 shows that the optimal backscatter antenna set for the case of $M = 2$ is composed of the antennas with the largest channel modulus and the smallest channel modulus, i.e., $\mathcal{S}_{opt} = \{1, 4\}$, which corroborates *Proposition* 2. Fig. 9 also shows that the optimal backscatter antenna set for the case of $M = 3$ is $\mathcal{S}_{opt} = \{1, 3, 4\}$, which, in turn, verifies our *Proposition* 3.

VI. Conclusion

In this paper, we have investigated the signal detection problem for ambient backscatter systems with multi-antenna tags that could perform energy harvesting and backscatter transmission simultaneously. More specifically, we have introduced a GLRT based detector and utilized the eigenvalues of the covariance matrix of the received signals at the reader to construct the decision statistic. The asymptotic threshold and detection probability of the detector have also been analyzed. Moreover, we have proposed a backscatter antenna selection method to maximize the detection probability. Finally, extensive simulations verified the effectiveness of the proposed GLRT based detector. The presented simulation results have verified that the selection of only two antennas provides the largest detection probability. It is worth noting that multi-antenna tags create a vast number of future research directions, such as the implementation of the more sophisticated coding schemes (e.g., space-time coding), the integration with the fifth generation (5G) of wireless networks [54]–[56], and the utilization of the artificial intelligence for backscatter communications [57], [58].

Appendix A
Proof of Theorem 3

Define the unknown parameter matrix as $\mathbf{\Phi} \in \mathbb{R}^{L\times L}$. The detection problem (7) can be parameterized as

$$\begin{cases} \mathcal{H}_0 : \mathbf{\Phi} = \mathbf{\Phi}_0, & B = 0, \\ \mathcal{H}_1 : \mathbf{\Phi} = \mathbf{\Phi}_1, & B = 1, \end{cases} \tag{61}$$

where $\mathbf{\Phi}_0 = \mathrm{diag}\{\underbrace{\varepsilon, \ldots, \varepsilon}_{L}\}$ and $\mathbf{\Phi}_1 = \tilde{\mathbf{C}}_1$. In total, there are L^2 unknown signal parameters, which agree with the number of the elements in $\tilde{\mathbf{C}}_1$.

Define $\mathbf{\Phi}_0$ and $\mathbf{\Phi}_1$ as $\left[(\boldsymbol{\rho}_1^0)^T, (\boldsymbol{\rho}_2^0)^T, \ldots, (\boldsymbol{\rho}_L^0)^T\right]^T$ and $\left[(\boldsymbol{\rho}_1^1)^T, (\boldsymbol{\rho}_2^1)^T, \ldots, (\boldsymbol{\rho}_L^1)^T\right]^T$, respectively, where $\boldsymbol{\rho}_l^0$ and $\boldsymbol{\rho}_l^1$ are the lth ($1 \le l \le L$) row of the unknown parameter matrices $\mathbf{\Phi}_0$ and $\mathbf{\Phi}_1$

$$\boldsymbol{\rho}_l^0 = [\underbrace{0, \ldots, 0}_{l-1}, \varepsilon, \underbrace{0, \ldots, 0}_{L-l}], \ \boldsymbol{\rho}_l^1 = [\underbrace{0, \ldots, 0}_{l-1}, [\tilde{\mathbf{C}}_1]_{l,l}, \underbrace{0, \ldots, 0}_{L-l}]. \tag{62}$$

Let us vectorize the matrices $\mathbf{\Phi}_0$ and $\mathbf{\Phi}_1$ as $\boldsymbol{\phi}_0 = [\boldsymbol{\rho}_1^0, \boldsymbol{\rho}_2^0, \ldots, \boldsymbol{\rho}_L^0]^T$ and $\boldsymbol{\phi}_1 = [\boldsymbol{\rho}_1^1, \boldsymbol{\rho}_2^1, \ldots, \boldsymbol{\rho}_L^1]^T$, respectively. Note that the PDFs of the received signals $\mathbf{y}$ under $\mathcal{H}_0$ and $\mathcal{H}_1$ are similar while the values of the unknown parameter vector $\boldsymbol{\phi}_0$ under $\mathcal{H}_0$ and that of the vector $\boldsymbol{\phi}_1$ under $\mathcal{H}_1$ are different. The unknown parameter vector is defined as $\boldsymbol{\phi} \in \mathbb{R}^{L^2\times 1}$. The detection problem (61) can be further simplified as

$$\begin{cases} \mathcal{H}_0 : \boldsymbol{\phi} = \boldsymbol{\phi}_0, & B = 0, \\ \mathcal{H}_1 : \boldsymbol{\phi} \neq \boldsymbol{\phi}_0, & B = 1. \end{cases} \tag{63}$$

The PDF of $\mathbf{y}$ is defined as $p(\mathbf{y}; \boldsymbol{\phi})$. To decide to accept the null hypothesis $\mathcal{H}_0$ or reject it in favor of alternative

hypothesis $\mathcal{H}_1$, the test statistic of the hypothesis testing problem (63) is given by [46]

$$T_{\mathrm{GLRT}} = \frac{p(\mathbf{y};\widehat{\boldsymbol{\phi}}_1)}{p(\mathbf{y};\boldsymbol{\phi}_0)}. \tag{64}$$

As stated in Section III-B, our goal is to derive the asymptotic distribution of the GLRT statistic T_{GLRT} to determine the decision threshold and construct the decision rule. To this end, we first notice the fact [48] that the estimation $\widehat{\boldsymbol{\phi}}_1$ attains the Cramer-Rao lower bound if

$$\frac{\partial \ln p(\mathbf{y};\boldsymbol{\phi})}{\partial \boldsymbol{\phi}} = \mathbf{I}(\boldsymbol{\phi})(\widehat{\boldsymbol{\phi}}_1 - \boldsymbol{\phi}) \tag{65}$$

$$= \left[\frac{\partial \ln p(\mathbf{y};\boldsymbol{\phi})}{\partial [\boldsymbol{\phi}]_1}, \frac{\partial \ln p(\mathbf{y};\boldsymbol{\phi})}{\partial [\boldsymbol{\phi}]_2}, \ldots, \frac{\partial \ln p(\mathbf{y};\boldsymbol{\phi})}{\partial [\boldsymbol{\phi}]_{L^2}}\right]^T, \tag{66}$$

where $\mathbf{I}(\boldsymbol{\phi})$ is the Fisher information matrix [46] and

$$\frac{\partial \ln p(\mathbf{y};\boldsymbol{\phi})}{\partial [\boldsymbol{\phi}]_i} = \sum_{j=1}^{L^2} [\mathbf{I}(\boldsymbol{\phi})]_{i,j}([\widehat{\boldsymbol{\phi}}_1]_j - [\boldsymbol{\phi}]_j). \tag{67}$$

Replacing $[\mathbf{I}(\boldsymbol{\phi})]_{i,j}$ with its first-order Taylor expansion $[\mathbf{I}(\widehat{\boldsymbol{\phi}}_1)]_{i,j} + \frac{\partial [\mathbf{I}(\boldsymbol{\phi})]_{i,j}}{\partial \boldsymbol{\phi}}\Big|^T_{\boldsymbol{\phi}=\widehat{\boldsymbol{\phi}}_1}(\boldsymbol{\phi} - \widehat{\boldsymbol{\phi}}_1)$, we rewrite (67) as

$$\frac{\partial \ln p(\mathbf{y};\boldsymbol{\phi})}{\partial [\boldsymbol{\phi}]_i} = \sum_{j=1}^{L^2} [\mathbf{I}(\widehat{\boldsymbol{\phi}}_1)]_{i,j}([\widehat{\boldsymbol{\phi}}_1]_j - [\boldsymbol{\phi}]_j) + \sum_{j=1}^{L^2} \frac{\partial [\mathbf{I}(\boldsymbol{\phi})]_{i,j}}{\partial \boldsymbol{\phi}}\Big|^T_{\boldsymbol{\phi}=\widehat{\boldsymbol{\phi}}_1}(\boldsymbol{\phi} - \widehat{\boldsymbol{\phi}}_1)([\widehat{\boldsymbol{\phi}}_1]_j - [\boldsymbol{\phi}]_j). \tag{68}$$

When $N \to \infty$, the second term in (68) can be neglected. Substituting the simplified element (68) into (65), the equation (65) can be further written as

$$\frac{\partial \ln p(\mathbf{y};\boldsymbol{\phi})}{\partial \boldsymbol{\phi}} = \mathbf{I}(\widehat{\boldsymbol{\phi}}_1)(\widehat{\boldsymbol{\phi}}_1 - \boldsymbol{\phi}) = \Bigg[\sum_{j=1}^{L^2} [\mathbf{I}(\widehat{\boldsymbol{\phi}}_1)]_{1,j}([\widehat{\boldsymbol{\phi}}_1]_j - [\boldsymbol{\phi}]_j), \sum_{j=1}^{L^2} [\mathbf{I}(\widehat{\boldsymbol{\phi}}_1)]_{2,j}([\widehat{\boldsymbol{\phi}}_1]_j - [\boldsymbol{\phi}]_j), \ldots, \sum_{j=1}^{L^2} [\mathbf{I}(\widehat{\boldsymbol{\phi}}_1)]_{L^2,j}([\widehat{\boldsymbol{\phi}}_1]_j - [\boldsymbol{\phi}]_j)\Bigg]^T. \tag{69}$$

Next, integrating the first derivative $\frac{\partial \ln p(\mathbf{y};\boldsymbol{\phi})}{\partial \boldsymbol{\phi}}$ over $\boldsymbol{\phi}$ produces

$$\int \frac{\partial \ln p(\mathbf{y};\boldsymbol{\phi})}{\partial \boldsymbol{\phi}} \mathrm{d}\boldsymbol{\phi} = \int \mathbf{I}(\widehat{\boldsymbol{\phi}}_1)(\widehat{\boldsymbol{\phi}}_1 - \boldsymbol{\phi})\mathrm{d}\boldsymbol{\phi} = -\frac{1}{2}(\widehat{\boldsymbol{\phi}}_1 - \boldsymbol{\phi})^T \mathbf{I}(\widehat{\boldsymbol{\phi}}_1)(\widehat{\boldsymbol{\phi}}_1 - \boldsymbol{\phi}) + c, \tag{70}$$

where c is a constant and defined as $\ln p(\mathbf{y};\widehat{\boldsymbol{\phi}}_1)$ in our work. As a consequence, the asymptotic form of the PDF is obtained as

$$p(\mathbf{y};\boldsymbol{\phi}) = \exp\left[-\frac{1}{2}(\widehat{\boldsymbol{\phi}}_1 - \boldsymbol{\phi})^T \mathbf{I}(\widehat{\boldsymbol{\phi}}_1)(\widehat{\boldsymbol{\phi}}_1 - \boldsymbol{\phi}) + c\right] = p(\mathbf{y};\widehat{\boldsymbol{\phi}}_1)\exp\left[-\frac{1}{2}(\widehat{\boldsymbol{\phi}}_1 - \boldsymbol{\phi})^T \mathbf{I}(\widehat{\boldsymbol{\phi}}_1)(\widehat{\boldsymbol{\phi}}_1 - \boldsymbol{\phi})\right]. \tag{71}$$

Consequently, substituting $\boldsymbol{\phi}_0$ into (71) and then substituting $p(\mathbf{y};\boldsymbol{\phi}_0)$ into (64) yields the GLRT statistic as

$$T_{\mathrm{GLRT}} = \exp\left[\frac{1}{2}(\widehat{\boldsymbol{\phi}}_1 - \boldsymbol{\phi}_0)^T \mathbf{I}(\widehat{\boldsymbol{\phi}}_1)(\widehat{\boldsymbol{\phi}}_1 - \boldsymbol{\phi}_0)\right]. \tag{72}$$

Define $T_s = \ln T_{\mathrm{GLRT}} = \frac{1}{2}(\widehat{\boldsymbol{\phi}}_1 - \boldsymbol{\phi}_0)^T \mathbf{I}(\widehat{\boldsymbol{\phi}}_1)(\widehat{\boldsymbol{\phi}}_1 - \boldsymbol{\phi}_0)$. As $N \to \infty$, we have [46]

$$2T_s = \begin{cases} (\widehat{\boldsymbol{\phi}}_1 - \boldsymbol{\phi}_0)^T \mathbf{I}(\boldsymbol{\phi}_0)(\widehat{\boldsymbol{\phi}}_1 - \boldsymbol{\phi}_0), & \text{under } \mathcal{H}_0, \\ (\widehat{\boldsymbol{\phi}}_1 - \boldsymbol{\phi}_0)^T \mathbf{I}(\boldsymbol{\phi}_1)(\widehat{\boldsymbol{\phi}}_1 - \boldsymbol{\phi}_0), & \text{under } \mathcal{H}_1. \end{cases} \tag{73}$$

It can be readily checked that $\widehat{\boldsymbol{\phi}}_1 \sim \mathcal{N}(\boldsymbol{\phi}_0, \mathbf{I}^{-1}(\boldsymbol{\phi}_0))$ when under $\mathcal{H}_0$, while $\widehat{\boldsymbol{\phi}}_1 \sim \mathcal{N}(\boldsymbol{\phi}_1, \mathbf{I}^{-1}(\boldsymbol{\phi}_1))$ when under $\mathcal{H}_1$. In consequence,

$$\widehat{\boldsymbol{\phi}}_1 - \boldsymbol{\phi}_0 \sim \begin{cases} \mathcal{N}(0, \mathbf{I}^{-1}(\boldsymbol{\phi}_0)), & \text{under } \mathcal{H}_0, \\ \mathcal{N}(\boldsymbol{\phi}_1 - \boldsymbol{\phi}_0, \mathbf{I}^{-1}(\boldsymbol{\phi}_1)), & \text{under } \mathcal{H}_1. \end{cases} \tag{74}$$

Finally, from (73) and (74), we obtain the distribution of the statistic $2T_s$ (73) as (44). In other words, under $\mathcal{H}_0$, $2T_s$ follows the chi-squared distribution with the degrees of freedom L^2, and under $\mathcal{H}_1$, it follows the non-central chi-squared distribution with the degrees of freedom L^2 and the noncentrality parameter

$$\tau = (\boldsymbol{\phi}_1 - \boldsymbol{\phi}_0)^T \mathbf{I}(\boldsymbol{\phi}_0)(\boldsymbol{\phi}_1 - \boldsymbol{\phi}_0), \tag{75}$$

It is clear that the unknown parameter vector $\boldsymbol{\phi}_0$ is only related with ε. In such a way, we replace $\mathbf{I}(\boldsymbol{\phi}_0)$ with $\mathbf{I}(\varepsilon)$, which is computed by

$$\mathbf{I}(\varepsilon) = -\mathbb{E}\left(\frac{\partial^2 \ln p(\mathbf{y};\mathbf{C}_0,\mathcal{H}_0)}{\partial \varepsilon^2}\right) = \frac{N}{\varepsilon^2}. \tag{76}$$

Then the noncentrality parameter τ can be further derived as

$$\tau = (\boldsymbol{\phi}_1 - \boldsymbol{\phi}_0)^T \frac{\mathbf{I}(\varepsilon)}{L^2}(\boldsymbol{\phi}_1 - \boldsymbol{\phi}_0) = \frac{N}{\varepsilon^2 L^2}\sum_{m=1}^{M} l_m \delta_m^2, \tag{77}$$

where $\delta_m = (|\mu_{\kappa_m}|^2 - |h|^2)P_s$.

Fig. 10 schematically presents the PDF curves of the chi-squared distribution $\chi^2_{L^2}$, the noncentrality chi-squared distribution $\chi'^2_{L^2}(\tau)$, and the statistic $2T_s$ under $\mathcal{H}_0$ and $\mathcal{H}_1$, respectively. Clearly, the PDF of the statistic $2T_s$ under $\mathcal{H}_0$ ($\mathcal{H}_1$) is close to the distribution $\chi^2_{L^2}$ ($\chi'^2_{L^2}(\tau)$).

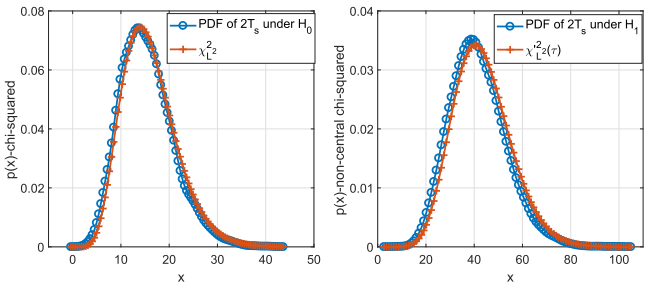

(a) Under $\mathcal{H}_0$ (b) Under $\mathcal{H}_1$

Fig. 10. Asymptotic distribution of the GLRT statistic $2T_s$ when SNR $= -10$ dB.

APPENDIX B
PROOF OF PROPOSITION 1

In the case that only one selected antenna backscatters all RF signals, i.e., $M = 1$, the hypothesis test (7) is simplified as

$$\begin{cases} \mathcal{H}_0 : \mathbf{y} = h\mathbf{x} + \boldsymbol{\omega}, & B = 0, \\ \mathcal{H}_1 : \mathbf{y} = \mu_\kappa \mathbf{x} + \boldsymbol{\omega}, & B = 1, \end{cases} \tag{78}$$

where κ indicates that the κth ($1 \leq \kappa \leq K$) antenna is selected. In that way, the received signals $\mathbf{y}$ follow the distribution (10) under $\mathcal{H}_1$, i.e., $\mathbf{y} \sim \mathcal{CN}(\mathbf{0}, \mathbf{C}_1)$, where the covariance matrix $\mathbf{C}_1$ is reduced to $(|\mu_\kappa|^2 P_s + \sigma_0^2)\mathbf{I}_N$.

Let $\zeta = |\mu_\kappa|^2 P_s + \sigma_0^2$. The LLF (34) can be simplified as

$$\ln p(\mathbf{y}; \mathbf{C}_1, \mathcal{H}_1) = -N \ln \pi - N \ln \zeta - \frac{\mathbf{y}^T \mathbf{y}}{\zeta}. \tag{79}$$

Similar to the derivation of the MLE of ε, we obtain the MLE of ζ through taking derivative of the LLF (79). Thus, the MLE $\hat{\zeta}$ is $\frac{\mathbf{y}^T\mathbf{y}}{N}$, and the MLE $\widehat{\mathbf{C}}_1$ is $\hat{\zeta}\mathbf{I}_N$. As a result, the log-GLRT statistic (39) is

$$\begin{aligned} T_s &= \ln p(\mathbf{y}; \widehat{\mathbf{C}}_1, \mathcal{H}_1) - \ln p(\mathbf{y}; \widehat{\mathbf{C}}_0, \mathcal{H}_0) \\ &= N \ln(\hat{\varepsilon}) + \mathbf{y}^T (\hat{\varepsilon}\mathbf{I}_N)^{-1} \mathbf{y} - N \ln\left(\hat{\zeta}\right) - \mathbf{y}^T \left(\hat{\zeta}\mathbf{I}_N\right)^{-1} \mathbf{y} \\ &= 0. \end{aligned} \tag{80}$$

In this case, GLRT fails to find an efficient statistic which verifies our Proposition 1.

APPENDIX C
PROOF OF PROPOSITION 3

Define a positive integer $\tilde{k}$, which satisfies

$$\tilde{k} = \underset{1 \leq k \leq K}{\arg\min} \{|\mu_k| \big| |\mu_1|^2 - |\mu_k|^2 < |\mu_k|^2 - |\mu_K|^2\}. \tag{81}$$

The whole candidate antenna set $\mathcal{A}$ can be divided into two sets

$$\mathcal{A}_1 = \{1, 2, \ldots, \tilde{k}\},\ \mathcal{A}_2 = \{\tilde{k}+1, \tilde{k}+2, \ldots, K\}. \tag{82}$$

When $M = 3$, i.e., the candidate backscatter antenna set is $\mathcal{S} = \{\kappa_1, \kappa_2, \kappa_3\}$, we first notice that $\sigma_1^2 > \sigma_2^2 > \sigma_3^2$. We assume that

$$\begin{aligned} s_1 &= l_2\sigma_2^2 + l_3\sigma_3^2,\ s_2 = l_1\sigma_1^2 + l_2\sigma_2^2, \\ p_1 &= (\sigma_2^2)^{l_2}(\sigma_3^2)^{l_3},\ p_2 = (\sigma_1^2)^{l_1}(\sigma_2^2)^{l_2}. \end{aligned} \tag{83}$$

Similarly to (59) and (60), we calculate the derivative of the statistic T_{s1} (57) with respect to σ_1^2 and σ_3^2, respectively, which are given by

$$\begin{aligned} \frac{\partial T_{s1}}{\partial \sigma_1^2} &= \frac{l_1}{L}\left[(\sigma_1^2)^{l_1} p_1\right]^{-\frac{1}{L}} \left(1 - \frac{l_1\sigma_1^2 + s_1}{L\sigma_1^2}\right), \\ \frac{\partial T_{s1}}{\partial \sigma_3^2} &= \frac{l_3}{L}\left[p_2(\sigma_3^2)^{l_3}\right]^{-\frac{1}{L}} \left(1 - \frac{s_2 + l_3\sigma_3^2}{L\sigma_3^2}\right). \end{aligned} \tag{84}$$

Since $l_1\sigma_1^2 + s_1 < L\sigma_1^2$ and $s_2 + l_3\sigma_3^2 > L\sigma_3^2$, the statistic T_{s1} is a monotonous increasing function of σ_1^2 (or $|\mu_{\kappa_1}|^2$), while a monotonous decreasing function of σ_3^2 (or $|\mu_{\kappa_3}|^2$). To maximize the detection probability, we first set $|\mu_{\kappa_1}| = |\mu_1|$ and $|\mu_{\kappa_3}| = |\mu_K|$. Then, by taking derivative of T_{s1} with respect to σ_2^2, we have

$$\frac{\partial T_{s1}}{\partial \sigma_2^2} = \frac{l_2}{L}\left[\prod_{m=1}^{3} (\sigma_m^2)^{l_m}\right]^{-\frac{1}{L}} \left(1 - \frac{\sum_{m=1}^{3} l_m\sigma_m^2}{L\sigma_2^2}\right). \tag{85}$$

It can be readily checked from (33) that

$$\begin{aligned} &\sum_{m=1}^{3} l_m\sigma_m^2 - L\sigma_2^2 \\ &\quad = l_1(|\mu_1|^2 - |\mu_{\kappa_2}|^2)P_s + l_3(|\mu_K|^2 - |\mu_{\kappa_2}|^2)P_s. \end{aligned} \tag{86}$$

There exist three cases:

- $l_1 < l_3$: in this case, we choose the antenna κ_2 from $\mathcal{A}_1$. Then the item (86) is smaller than zero and the first derivative (85) is greater than zero. As a result, the statistic T_{s1} is strictly increasing with respect to $|\mu_{\kappa_2}|^2$, and we set $\kappa_2 = 2$.
- $l_1 > l_3$: in this case, we choose the antenna κ_2 from $\mathcal{A}_2$. Accordingly, the item (86) is greater than zero and the first derivative (85) is smaller than zero. Therefore, the statistic T_{s1} is strictly decreasing with respect to $|\mu_{\kappa_2}|^2$, and we set $\kappa_2 = K - 1$.
- $l_1 = l_3$: in this case, the item (86) is smaller than zero (i.e., the statistic T_{s1} is a monotonous increasing function of $|\mu_{\kappa_2}|^2$) when $\kappa_2 \in \mathcal{A}_1$, while is greater than zero (i.e., the statistic T_{s1} is a monotonous decreasing function of $|\mu_{\kappa_2}|^2$) when $\kappa_2 \in \mathcal{A}_2$. As a result, we set $\kappa_2 = 2$ if $\kappa_2 \in \mathcal{A}_1$, and set $\kappa_2 = K - 1$ if $\kappa_2 \in \mathcal{A}_2$.

APPENDIX D
PROOF OF PROPOSITION 4

When selecting three backscatter antennas, i.e., $M = 3$, we denote the candidate backscatter antenna set as $\mathcal{S} = \{\kappa_1, \kappa_2, \kappa_3\}$. For simplification, we set $l_1 = l_2 = l_3$. It has been proved in Appendix C that the backscatter antennas κ_1 and κ_3 should be the antennas with the largest channel modulus and the smallest channel modulus, respectively, i.e., $\kappa_1 = 1$ and $\kappa_3 = K$. The left problem is to determine which antenna is the optimal backscatter antenna κ_2. There exist two possible choices: $\kappa_2 \in \mathcal{A}_1$ or $\kappa_2 \in \mathcal{A}_2$, where $\mathcal{A}_1$ and $\mathcal{A}_2$ have been defined in (82).

In the case of $\kappa_2 \in \mathcal{A}_1$, it can be readily checked from Appendix C that the statistic T_{s1} is monotonously increasing with respect to $|\mu_{\kappa_2}|^2$. Therefore, the maximum detection probability is achieved if the channel modulus of the κ_2th antenna is equal to the largest channel modulus $|\mu_1|$, i.e., $\kappa_2 = 1$. Similarly, if we choose κ_2 from $\mathcal{A}_2$, the statistic T_{s1} is monotonously decreasing with respect to $|\mu_{\kappa_2}|^2$. Thus, the detection probability is maximized when the channel modulus of the κ_2th antenna is equal to the smallest channel modulus $|\mu_K|$, i.e., $\kappa_2 = K$.

In conclusion, we obtain the largest detection probability if the optimal backscatter antenna set is $\mathcal{S}_{opt} = \{1, 1, K\}$ or $\mathcal{S}_{opt} = \{1, K, K\}$, which indicates that the detection performance of selecting only two antennas ($M = 2$) is better than that of selecting three antennas ($M = 3$).

REFERENCES

[1] N. Van Huynh, D. T. Hoang, X. Lu, D. Niyato, P. Wang, and D. I. Kim, "Ambient backscatter communications: A contemporary survey," *IEEE Commun. Surveys Tuts.*, vol. 20, no. 4, pp. 2889–2922, 4th Quart., 2018.

[2] V. Liu, A. Parks, V. Talla, S. Gollakota, D. Wetherall, and J. Smith, "Ambient backscatter: Wireless communication out of thin air," in *Proc. ACM SIGCOMM*, Hong Kong, Aug. 2013, pp. 39–50.

[3] C. Boyer and S. Roy, "Backscatter communication and RFID: Coding, energy, and MIMO analysis," *IEEE Trans. Commun.*, vol. 62, no. 3, pp. 770–785, Mar. 2014.

[4] B. Kellogg, A. Parks, S. Gollakota, J. R. Smith, and D. Wetherall, "Wi-Fi backscatter: Internet connectivity for RF-powered devices," in *Proc. ACM SIGCOMM*, Chicago, IL, USA, Aug. 2014, pp. 607–618.

[5] D. Bharadia, K. R. Joshi, M. Kotaru, and S. Katti, "BackFi: High throughput WiFi backscatter," in *Proc. ACM SIGCOMM*, London, U.K., Aug. 2015, pp. 283–296.

[6] A. N. Parks, A. Liu, S. Gollakota, and J. R. Smith, "Turbocharging ambient backscatter communication," in *Proc. ACM SIGCOMM*, Chicago, IL, USA, Aug. 2014, pp. 619–630.

[7] B. Kellogg, V. Talla, S. Gollakota, and J. R. Smith, "Passive Wi-Fi: Bringing low power to Wi-Fi transmissions," in *Proc. NSDI*, Santa Clara, CA, USA, Mar. 2016, pp. 151–164.

[8] A. Wang, V. Iyer, V. Talla, J. R. Smith, and S. Gollakota, "FM backscatter: Enabling connected cities and smart fabrics," in *Proc. NSDI*, Boston, MA, USA, Mar. 2017, pp. 243–258.

[9] S. Ma, G. Wang, R. Fan, and C. Tellambura, "Blind channel estimation for ambient backscatter communication systems," *IEEE Commun. Lett.*, vol. 22, no. 6, pp. 1296–1299, Jun. 2018.

[10] G. Wang, F. Gao, R. Fan, and C. Tellambura, "Ambient backscatter communication systems: Detection and performance analysis," *IEEE Trans. Commun.*, vol. 64, no. 11, pp. 4836–4846, Nov. 2016.

[11] J. Qian, F. Gao, G. Wang, S. Jin, and H. Zhu, "Noncoherent detections for ambient backscatter system," *IEEE Trans. Wireless Commun.*, vol. 16, no. 3, pp. 1412–1422, Mar. 2017.

[12] J. Qian, F. Gao, G. Wang, S. Jin, and H. Zhu, "Semi-coherent detection and performance analysis for ambient backscatter system," *IEEE Trans. Commun.*, vol. 65, no. 12, pp. 5266–5279, Dec. 2017.

[13] S. Ma, G. Wang, Y. Wang, and Z. Zhao, "Signal ratio detection and approximate performance analysis for ambient backscatter communication systems with multiple receiving antennas," *Mobile Netw. Appl.*, vol. 23, no. 6, pp. 1478–1486, Dec. 2018.

[14] G. Yang, Q. Zhang, and Y.-C. Liang, "Cooperative ambient backscatter communications for green Internet-of-Things," *IEEE Internet Things J.*, vol. 5, no. 2, pp. 1116–1130, Apr. 2018.

[15] C. Chen, G. Wang, R. He, F. Gao, and Z. Li, "Semi-blind detection of ambient backscatter signals from multiple-antenna tags," in *Proc. APCC*, Ningbo, China, Nov. 2018, pp. 570–575.

[16] C. Xing, S. Ma, Z. Fei, Y.-C. Wu, and H. V. Poor, "A general robust linear transceiver design for multi-hop amplify-and-forward MIMO relaying systems," *IEEE Trans. Signal Process.*, vol. 61, no. 5, pp. 1196–1209, Mar. 2013.

[17] C. Xing, Y. Ma, Y. Zhou, and F. Gao, "Transceiver optimization for multi-hop communications with per-antenna power constraints," *IEEE Trans. Signal Process.*, vol. 64, no. 6, pp. 1519–1534, Mar. 2016.

[18] Q. Tao, C. Zhong, H. Lin, and Z. Zhang, "Symbol detection of ambient backscatter systems with Manchester coding," *IEEE Trans. Wireless Commun.*, vol. 17, no. 6, pp. 4028–4038, Jun. 2018.

[19] X. Zhou, G. Wang, Y. Wang, and J. Cheng, "An approximate BER analysis for ambient backscatter communication systems with tag selection," *IEEE Access*, vol. 5, pp. 22552–22558, 2017.

[20] I. Krikidis, "Retrodirective large antenna energy beamforming in backscatter multi-user networks," *IEEE Wireless Commun. Lett.*, vol. 7, no. 4, pp. 678–681, Aug. 2018.

[21] C. Psomas and I. Krikidis, "Backscatter communications for wireless powered sensor networks with collision resolution," *IEEE Wireless Commun. Lett.*, vol. 6, no. 5, pp. 650–653, Oct. 2017.

[22] C. Psomas and I. Krikidis, "Collision avoidance in wireless powered sensor networks with backscatter communications," in *Proc. SPAWC*, Sapporo, Japan, Jul. 2017, pp. 1–5.

[23] D. Li and Y.-C. Liang, "Adaptive ambient backscatter communication systems with MRC," *IEEE Trans. Veh. Technol.*, vol. 67, no. 12, pp. 12352–12357, Dec. 2018.

[24] D. Li, W. Peng, and Y.-C. Liang, "Hybrid ambient backscatter communication systems with harvest-then-transmit protocols," *IEEE Access*, vol. 6, pp. 45288–45298, 2018.

[25] K. Han and K. Huang, "Wirelessly powered backscatter communication networks: Modeling, coverage, and capacity," *IEEE Trans. Wireless Commun.*, vol. 16, no. 4, pp. 2548–2561, Apr. 2017.

[26] S. Gong, X. Huang, J. Xu, W. Liu, P. Wang, and D. Niyato, "Backscatter relay communications powered by wireless energy beamforming," *IEEE Trans. Commun.*, vol. 66, no. 7, pp. 3187–3200, Jul. 2018.

[27] Y. Zhou, H. Liu, Z. Pan, L. Tian, J. Shi, and G. Yang, "Two-stage cooperative multicast transmission with optimized power consumption and guaranteed coverage," *IEEE J. Sel. Areas Commun.*, vol. 32, no. 2, pp. 274–284, Feb. 2014.

[28] V. Garcia, Y. Zhou, and J. Shi, "Coordinated multipoint transmission in dense cellular networks with user-centric adaptive clustering," *IEEE Trans. Wireless Commun.*, vol. 13, no. 8, pp. 4297–4308, Aug. 2014.

[29] L. Liu, Y. Zhou, L. Tian, and J. Shi, "CPC-based backward-compatible network access for LTE cognitive radio cellular networks," *IEEE Commun. Mag.*, vol. 53, no. 7, pp. 93–99, Jul. 2015.

[30] G. Yang, Y.-C. Liang, R. Zhang, and Y. Pei, "Modulation in the air: Backscatter communication over ambient OFDM carrier," *IEEE Trans. Commun.*, vol. 66, no. 3, pp. 1219–1233, Mar. 2018.

[31] D. Darsena, G. Gelli, and F. Verde, "Modeling and performance analysis of wireless networks with ambient backscatter devices," *IEEE Trans. Commun.*, vol. 65, no. 4, pp. 1797–1814, Jan. 2017.

[32] W. Zhao, G. Wang, S. Atapattu, C. Tellambura, and H. Guan, "Outage analysis of ambient backscatter communication systems," *IEEE Commun. Lett.*, vol. 22, no. 8, pp. 1736–1739, Aug. 2018.

[33] Y. Jing and B. Hassibi, "Distributed space-time coding in wireless relay networks," *IEEE Trans. Wireless Commun.*, vol. 5, no. 12, pp. 3524–3536, Dec. 2006.

[34] J. D. Griffin and G. D. Durgin, "Gains for RF tags using multiple antennas," *IEEE Trans. Antennas Propag.*, vol. 56, no. 2, pp. 563–570, Feb. 2008.

[35] C. Boyer and S. Roy, "Space time coding for backscatter RFID," *IEEE Trans. Wireless Commun.*, vol. 12, no. 5, pp. 2272–2280, May 2013.

[36] X. Lu, D. Niyato, H. Jiang, D. I. Kim, Y. Xiao, and Z. Han, "Ambient backscatter assisted wireless powered communications," *IEEE Wireless Commun.*, vol. 25, no. 2, pp. 170–177, Apr. 2018.

[37] J. Kimionis, A. Bletsas, and J. N. Sahalos, "Increased range bistatic scatter radio," *IEEE Trans. Commun.*, vol. 62, no. 3, pp. 1091–1104, Mar. 2014.

[38] C. Xu, L. Yang, and P. Zhang, "Practical backscatter communication systems for battery-free Internet of Things: A tutorial and survey of recent research," *IEEE Signal Process. Mag.*, vol. 35, no. 5, pp. 16–27, Sep. 2018.

[39] D. Niyato, D. I. Kim, M. Maso, and Z. Han, "Wireless powered communication networks: Research directions and technological approaches," *IEEE Wireless Commun.*, vol. 24, no. 6, pp. 88–97, Dec. 2017.

[40] A. P. Sample, D. J. Yeager, P. S. Powledge, A. V. Mamishev, and J. R. Smith, "Design of an RFID-based battery-free programmable sensing platform," *IEEE Trans. Instrum. Meas.*, vol. 57, no. 11, pp. 2608–2615, Nov. 2008.

[41] J. R. Smith, A. P. Sample, P. S. Powledge, S. Roy, and A. Mamishev, "A wirelessly-powered platform for sensing and computation," in *Proc. UbiComp*, 2006, pp. 495–506.

[42] X. Lu, P. Wang, D. Niyato, D. I. Kim, and Z. Han, "Wireless networks with RF energy harvesting: A contemporary survey," *IEEE Commun. Surveys Tuts.*, vol. 17, no. 2, pp. 757–789, 2nd Quart., 2015.

[43] T. Cui and C. Tellambura, "Joint data detection and channel estimation for OFDM systems," *IEEE Trans. Commun.*, vol. 54, no. 4, pp. 670–679, Apr. 2006.

[44] G. Wang, F. Gao, Y.-C. Wu, and C. Tellambura, "Joint CFO and channel estimation for OFDM-based two-way relay networks," *IEEE Trans. Wireless Commun.*, vol. 10, no. 2, pp. 456–465, Feb. 2011.

[45] G. Wang, F. Gao, W. Chen, and C. Tellambura, "Channel estimation and training design for two-way relay networks in time-selective fading environments," *IEEE Trans. Wireless Commun.*, vol. 10, no. 8, pp. 2681–2691, Aug. 2011.

[46] S. M. Kay, *Fundamentals of Statistical Signal Processing: Detection Theory*. Upper Saddle River, NJ, USA: Prentice-Hall, 1998.

[47] R. Zhang, T. J. Lim, Y.-C. Liang, and Y. Zeng, "Multi-antenna based spectrum sensing for cognitive radios: A GLRT approach," *IEEE Trans. Commun.*, vol. 58, no. 1, pp. 84–88, Jan. 2010.

[48] S. M. Kay, *Fundamentals of Statistical Signal Processing: Estimation Theory*. Upper Saddle River, NJ, USA: Prentice-Hall, 1993.

[49] M. Abramowitz and I. A. Stegun, *Handbook of Mathematical Functions With Formulas, Graphs, and Mathematical Tables*. New York, NY, USA: Dover, 1972.

[50] S. Atapattu, C. Tellambura, and H. Jiang, *Energy Detection for Spectrum Sensing in Cognitive Radio*. New York, NY, USA: Springer, 2014.
[51] G. W. Snedecor and W. G. Cochran, *Statistical Methods*, 8th ed. Ames, IA, USA: Iowa State Univ. Press, 1989.
[52] A. Papoulis and S. U. Pillai, *Probability, Random Variables, and Stochastic Processes*, 4th ed. New York, NY, USA: McGraw-Hill, 2002, ch. 7, pp. 278–279.
[53] C. Chen, G. Wang, F. Gao, Y. Eldar, and H. Guan, "Blind detection for ambient backscatter communication system with multiple-antenna tags," in *Proc. IEEE GLOBECOM*, Abu Dhabi, United Arab Emirates, Dec. 2018, pp. 206–212.
[54] Z. Zhang, X. Chai, K. Long, A. V. Vasilakos, and L. Hanzo, "Full duplex techniques for 5G networks: Self-interference cancellation, protocol design, and relay selection," *IEEE Commun. Mag.*, vol. 53, no. 5, pp. 128–137, May 2015.
[55] Z. Zhang, K. Long, and J. Wang, "Self-organization paradigms and optimization approaches for cognitive radio technologies: A survey," *IEEE Wireless Commun.*, vol. 20, no. 2, pp. 36–42, Apr. 2013.
[56] Z. Zhang, K. Long, J. Wang, and F. Dressler, "On swarm intelligence inspired self-organized networking: Its bionic mechanisms, designing principles and optimization approaches," *IEEE Commun. Surveys Tuts.*, vol. 16, no. 1, pp. 513–537, Feb. 2014.
[57] J. Zhang, P. Liu, F. Zhang, and Q. Song, "CloudNet: Ground-based cloud classification with deep convolutional neural network," *Geophys. Res. Lett.*, vol. 45, pp. 8665–8672, Aug. 2018.
[58] T.-H. Pham, N. Kyriazis, A. A. Argyros, and A. Kheddar, "Hand-object contact force estimation from markerless visual tracking," *IEEE Trans. Pattern Anal. Mach. Intell.*, vol. 40, no. 12, pp. 2883–2896, Dec. 2018.

Chen Chen received the B.Eng. degree in Internet of Things from Beijing Jiaotong University, Beijing, China, in 2016, where she is currently pursuing the Ph.D. degree with the School of Computer and Information Technology. Her research interests include signal processing in backscatter communication and wireless sensing.

Gongpu Wang received the B.Eng. degree in communication engineering from Anhui University, Hefei, Anhui, China, in 2001, the M.Sc. degree from the Beijing University of Posts and Telecommunications, Beijing, China, in 2004, and the Ph.D. degree from the University of Alberta, Edmonton, Canada, in 2011. From 2004 to 2007, he was an Assistant Professor with the School of Network Education, Beijing University of Posts and Telecommunications. He is currently a Full Professor with the School of Computer and Information Technology, Beijing Jiaotong University, China. His research interests include wireless communication, signal processing, artificial intelligence, and the Internet of Things.

Panagiotis D. Diamantoulakis (SM'18) received the Diploma (five years) and Ph.D. degrees from the Department of Electrical and Computer Engineering, Aristotle University of Thessaloniki (AUTH), Greece, in 2012 and 2017, respectively. From 2017 to 2019, he was a Visiting Post-Doctoral Researcher with the Key Laboratory of Information Coding and Transmission, Southwest Jiaotong University, China, and the Telecommunications Laboratory (LNT), Institute for Digital Communications (IDC), Friedrich-Alexander-Universität Erlangen-Nürnberg (FAU), Germany. Since 2017, he has been a Post-Doctoral Fellow with the Wireless Communications Systems Group (WCSG), AUTH. His current research interests include resource allocation in wireless communications, optimization theory and applications, game theory, non-orthogonal multiple access, and wireless power transfer. He also serves as an Editor for IEEE WIRELESS COMMUNICATIONS LETTERS, *Physical Communications* (Elsevier), and IEEE OPEN JOURNAL OF THE COMMUNICATIONS SOCIETY. He was also an Exemplary Reviewer of IEEE COMMUNICATIONS LETTERS in 2014 and IEEE TRANSACTIONS ON WIRELESS COMMUNICATIONS in 2017 (top 3% of reviewers).

Ruisi He (S'11–M'13–SM'17) received the B.E. and Ph.D. degrees from Beijing Jiaotong University (BJTU), Beijing, China, in 2009 and 2015, respectively. Since 2015, he has been with the State Key Laboratory of Rail Traffic Control and Safety, BJTU, where he has been a Full Professor since 2019. He has been a Visiting Scholar with the Georgia Institute of Technology, USA, the University of Southern California, USA, and the Université Catholique de Louvain, Belgium. He has authored or coauthored three books, three book chapters, and more than 100 journal and conference articles. He holds several patents. His research interests include measurement and modeling of wireless channels, machine learning and clustering analysis in communications, vehicular and high-speed railway communications, 5G massive MIMO, and high-frequency communication techniques.

George K. Karagiannidis (M'96–SM'03–F'14) was born in Pythagoreio, Samos Island, Greece. He received the University Diploma (5 years) and Ph.D. degrees in electrical and computer engineering from the University of Patras in 1987 and 1999, respectively.

From 2000 to 2004, he was a Senior Researcher with the Institute for Space Applications and Remote Sensing, National Observatory of Athens, Greece. In June 2004, he joined the faculty of Aristotle University of Thessaloniki, Greece, where he is currently a Professor with the Electrical and Computer Engineering Department and the Director of the Digital Telecommunications Systems and Networks Laboratory. He is also an Honorary Professor with South West Jiaotong University, Chengdu, China. He is also the author or coauthor of more than 500 technical articles published in scientific journals and presented at international conferences. He is also the author of the Greek edition of a book on *Telecommunications Systems* and coauthor of a book *Advanced Optical Wireless Communications Systems* (Cambridge Publications, 2012). His research interests are in the broad area of digital communications systems and signal processing, with emphasis on wireless communications, optical wireless communications, wireless power transfer and applications, communications for biomedical engineering, and stochastic processes in biology and wireless security.

Dr. Karagiannidis has been involved as the General Chair, the Technical Program Chair, and a member of the Technical Program Committees in several IEEE and non-IEEE conferences. In the past, he was an Editor of IEEE TRANSACTIONS ON COMMUNICATIONS and the *EURASIP Journal on Wireless Communications and Networks* and several times a Guest Editor of IEEE SELECTED AREAS IN COMMUNICATIONS. From 2012 to 2015, he was the Editor-in-Chief of IEEE COMMUNICATIONS LETTERS. He is one of the highly cited authors across all areas of electrical engineering, recognized from Clarivate Analytics as Web-of-Science Highly Cited Researcher in the five consecutive years 2015–2019.

Chintha Tellambura (F'11) received the B.Sc. degree in electronics and telecommunications from the University of Moratuwa, Sri Lanka, the M.Sc. degree in electronics from the Kings College, University of London, and the Ph.D. degree in electrical engineering from the University of Victoria, Canada.

He was with Monash University, Australia, from 1997 to 2002. Since 2002, he has been with the Department of Electrical and Computer Engineering, University of Alberta, where he is currently a Full Professor. He has authored or coauthored over 560 journal and conference articles, with an H-index of 73 (Google Scholar). He has supervised or co-supervised 66 M.Sc., Ph.D., and PDF trainees. His current research interests include cognitive radio, heterogeneous cellular networks, fifth-generation wireless networks, and machine learning algorithms. He was elected as a fellow of The Canadian Academy of Engineering in 2017. He was a recipient of the Best Paper Awards from IEEE International Conference on Communications (ICC) in 2012 and 2017. He is also the winner of the prestigious McCalla Professorship and the Killam Annual Professorship from the University of Alberta. He has served as an Editor for IEEE TRANSACTIONS ON COMMUNICATIONS from 1999 to 2012 and IEEE TRANSACTIONS ON WIRELESS COMMUNICATIONS from 2001 to 2007. He was an Area Editor of *Wireless Communications Systems and Theory* from 2007 to 2012.